

Higher measured than modeled ozone production at increased NO_x levels in the Colorado Front Range

Bianca Baier^{1,a,*}, William Brune¹, David Miller¹, Donald Blake², Russell Long³, Armin Wisthaler^{4,5}, Christopher Cantrell⁶, Alan Fried⁷, Brian Heikes⁸, Steven Brown^{9,10}, Erin McDuffie^{9,10,11}, Frank Flocke¹², Eric Apel¹², Lisa Kaser¹², and Andrew Weinheimer¹²

¹Department of Meteorology and Atmospheric Science, The Pennsylvania State University, University Park, PA, USA

²School of Physical Sciences, University of California, Irvine, CA, USA

³US EPA National Exposure Research Lab, Research Triangle Park, NC, USA

⁴Institute of Ion Physics and Applied Physics, University of Innsbruck, Austria

⁵Department of Chemistry, University of Oslo, Norway

⁶Department of Atmospheric and Oceanic Sciences, University of Colorado Boulder, Boulder, CO, USA

⁷INSTAAR, University of Colorado Boulder, Boulder, CO, USA

⁸Graduate School of Oceanography, The University of Rhode Island, Kingston, RI, USA

⁹Chemical Sciences Division, NOAA Earth System Research Laboratory, Boulder, CO, USA

¹⁰Department of Chemistry and Biochemistry, University of Colorado Boulder, Boulder, CO, USA

¹¹Cooperative Institute for Research in the Environmental Sciences, University of Colorado Boulder, Boulder, CO, USA

¹²Atmospheric Chemistry Observations and Modeling Laboratory, National Center for Atmospheric Research, Boulder, CO, USA

^anow at: Cooperative Institute for Research in the Environmental Sciences, University of Colorado Boulder, Boulder, CO, USA and Global Monitoring Division, NOAA Earth System Research Laboratory, Boulder, CO, USA

Correspondence to: Bianca Baier (bianca.baier@noaa.gov)

Abstract. Chemical models must correctly calculate the ozone formation rate, $P(\text{O}_3)$, to accurately predict ozone levels and to test mitigation strategies. However, air quality models can have large uncertainties in $P(\text{O}_3)$ calculations which can create uncertainties in ozone forecasts: especially during the summertime when $P(\text{O}_3)$ is high. One way to test mechanisms is to compare modeled $P(\text{O}_3)$ to direct measurements. During summer 2014, the Measurement of Ozone Production Sensor (MOPS) directly measured net $P(\text{O}_3)$ in Golden, CO, approximately 25 km west of Denver along the Colorado Front Range. Net $P(\text{O}_3)$ was compared to rates calculated by a photochemical box model that was constrained by measurements of other chemical species and that used a lumped chemical mechanism and a more explicit one. Median observed $P(\text{O}_3)$ was up to a factor of two higher than that modeled during early morning hours when nitric oxide (NO) levels were high and was similar to modeled for the rest of the day. While all possible interferences and offsets in this new method are not fully understood, simulations of these possible uncertainties cannot explain the observed $P(\text{O}_3)$ behavior. Furthermore, atmospheric peroxy (HO_2 and RO_2) radicals from unknown volatile organic compounds co-emitted with nitrogen oxides (NO_x) cannot fully explain the measured $P(\text{O}_3)$. This discrepancy observed between measured and modeled $P(\text{O}_3)$ is similar to those between measured and modeled peroxy radicals presented in this study and prior ones. If the MOPS accurately portrays atmospheric $P(\text{O}_3)$, then these results would imply that $P(\text{O}_3)$ in Golden, CO would be NO_x -sensitive for more of the day than what is calculated by models, extending the NO_x -sensitive $P(\text{O}_3)$ regime from the afternoon further into the morning. These results could affect ozone reduction strategies

for the region surrounding Golden and possibly other areas that are in non-attainment with national ozone regulations. Thus, it is important to continue the development of this direct ozone measurement technique to understand $P(O_3)$, especially under high NO_x regimes.

1 Introduction

- 5 Ground-level ozone (O_3) is a hazardous air pollutant abundant in cities and their surrounding areas. Awareness of its detrimental health effects on both humans and plants has led to the Clean Air Act of 1970 and the development of National Ambient Air Quality Standards (NAAQS) (Krupa and Manning, 1988; Bell et al., 2004; US EPA, 2013, 2016b). Air pollution regulatory policies based on these standards have been successful in reducing O_3 by approximately 32% in the United States since 1980. However, current O_3 levels are stabilizing and even increasing again in the western United States (US EPA, 2016a).
- 10 Understanding why these trends are occurring in areas despite more stringent emissions controls is crucial for further reduction of O_3 levels within the United States.

Boundary layer O_3 levels are dependent upon both chemical and meteorological processes described in the following equation:

$$\frac{\partial[O_3]}{\partial t} = P(O_3) + \frac{w_e \Delta O_3 - u_d [O_3]}{H} - \nabla \cdot (\mathbf{v}[O_3]), \quad (1)$$

- 15 where $\partial[O_3]/\partial t$ is the local O_3 time rate of change, $P(O_3)$ is the instantaneous net photochemical O_3 production rate, $(w_e \Delta O_3 - u_d [O_3])/H$ is the combined entrainment and deposition rate of O_3 in or out of the mixing layer of height H , and $\nabla \cdot (\mathbf{v}[O_3])$ is the O_3 advection rate. All of the physics, chemistry, and meteorology needed to solve this equation are included in chemical transport models (CTMs), which are used to design and test reduction strategies. For areas where local production is the dominant source of O_3 , the term in Eq. (1) that will reduce O_3 through local emissions control strategies is
- 20 $P(O_3)$. Thus, understanding and accurately calculating O_3 formation is crucial for its mitigation.

- Ozone formation chemistry has been well-documented for decades (Haagen-Smit et al., 1953; Finlayson-Pitts and Pitts, 1977; Seinfeld and Pandis, 2012; Calvert et al., 2015). The oxidation of volatile organic compounds (VOCs) by the hydroxyl radical (OH) produces hydroperoxy (HO_2) and organic peroxy (RO_2) radicals. These peroxy radicals react with nitrogen oxide (NO) to form nitrogen dioxide (NO_2), which is photolyzed to form new O_3 outside of the NO_x photostationary state (PSS):
- 25 a steady-state reaction sequence involving NO_x ($NO_2 + NO$) and O_3 . Thus, chemical O_3 production occurs through reactions with NO and peroxy radicals described in Eq. (2), where k denotes a bimolecular reaction rate coefficient. Equation (3) describes the chemical O_3 (or NO_2) destruction rate or rate of removal to reservoir species as the fraction of $O(^1D)$ molecules resulting from O_3 photolysis that react with H_2O to form OH; reactions of O_3 with HO_x ($HO_2 + OH$); the net production of peroxyacyl nitrates (PANs); the reaction of OH and NO_2 to form nitric acid (HNO_3); and O_3 loss through reactions with

alkenes and halogens. The net instantaneous O₃ production rate, P(O₃), is then defined as the difference between O₃ chemical production and loss rates in Eq. (4):

$$P_{chem} = k_{NO+HO_2}[NO][HO_2] + \sum_{i=1}^N k_{NO+RO_{2i}}[NO][RO_2]_i \quad (2)$$

$$L_{chem} = J_{O_3}f_{H_2O}[O_3] + k_{OH+O_3}[OH][O_3] + k_{HO_2+O_3}[HO_2][O_3] + P(PANs) + k_{OH+NO_2}[OH][NO_2] + L(O_3)_{alkenes} + L(O_3)_{halogens} \quad (3)$$

$$5 \quad P(O_3) = P_{chem} - L_{chem}. \quad (4)$$

Equations (2) and (3) illustrate the non-linear dependence of P(O₃) on both NO_x and the production of HO_x from VOC oxidation. That is, these chemical species are involved in both the production and destruction of O₃ molecules. According to the current understanding, increases in NO can cause P(O₃) to initially increase until NO_x levels are sufficiently high to react with OH, thereby removing HO_x and NO_x from the reaction system and decreasing P(O₃). Therefore, P(O₃) is largely
 10 dependent upon the cycling between HO_x and NO_x in the atmosphere; the exact NO_x level at which this crossover occurs is sensitive to the production rate of HO_x radicals (Jaegle et al., 1998; Trainer et al., 2000; Thornton et al., 2002; Ren et al., 2005). In a NO_x-sensitive regime, P(O₃) varies with the square root of P(HO_x) and decreases in NO_x are more effective in decreasing O₃ than decreases in VOCs. Conversely, in a VOC-sensitive regime, P(O₃) varies linearly with P(HO_x) and decreases in VOCs are more effective in decreasing O₃, while further NO_x decreases can act to increase O₃ (Kleinman et al., 1997; Seinfeld and
 15 Pandis, 2012). Therefore, if the sensitivity of P(O₃) to NO_x and VOCs is known, efficient O₃ mitigation strategies can be devised that target precursor emissions and more effectively reduce O₃ in polluted regions.

The gas-phase chemical mechanisms used in CTMs rely on a number of model input parameters to calculate P(O₃) such as measurements of inorganic and organic chemical species; temperature- and pressure-dependent reaction rates; photolysis frequencies; and product yields of reactions. As the chemical processes contributing to O₃ formation are vast, complex, and
 20 not fully quantified, it is difficult to portray atmospheric reactions in their entirety. Thus, mechanisms are simplified to describe the complex chemical state of the atmosphere. While inorganic chemistry is generally similar between reduced and more explicit mechanisms, differences in VOC aggregation schemes can create variance in modeled P(O₃), O₃, or other important O₃ precursor predictions (Jeffries and Tonnesen, 1994; Olson et al., 1997; Kuhn et al., 1998; Luecken et al., 1999; Dodge, 2000; Tonnesen and Dennis, 2000; Jimenez et al., 2003; Luecken et al., 2008; Chen et al., 2010).

25 The current understanding of O₃ production chemistry is not consistent with all observations. The production of O₃ is dictated by reactions between peroxy radicals (HO₂ and RO₂) and NO, but prior studies have shown that measured and modeled

peroxy radicals are not always in agreement. Stone et al. (2012) provide a synthesis of model-measurement HO₂ comparisons, noting that model agreement with measurements is variable in low-NO_x environments, but that models tend to underpredict HO₂ in urban, high-NO_x areas. Such studies in high-NO_x environments have shown that both zero-dimensional and three-dimensional modeled HO₂ – or the HO₂ to OH ratio – can be underestimated by up to a factor of ten at values of NO greater than a few parts per billion (Faloona et al., 2000; Martinez et al., 2003; Ren et al., 2003; Emmerson et al., 2005; Shirley et al., 2006; Emmerson et al., 2007; Kanaya et al., 2007, 2008; Dusanter et al., 2009; Chen et al., 2010; Sheehy et al., 2010; Ren et al., 2013; Czader et al., 2013; Brune et al., 2015; Griffith et al., 2016). For some studies, the maximum NO values were approximately 6 ppbv (Tan et al., 2017), so that the amount of model underestimation at high NO_x values was within measurement uncertainty. Other studies show good agreement between model and measured HO₂ in the morning with average diel NO less than 2 ppbv (Hofzumahaus et al., 2009), or indicate good average agreement between measured and modeled HO₂, but indicate morning model HO₂ underestimation on individual days (Lu et al., 2013). In 2010, an interference involving partial conversion of RO₂ to HO₂ was found in HO₂ measurements that use reagent NO to convert HO₂ to OH, so that measured HO₂ was overestimated (Fuchs et al., 2011). Since the publication of that discovery, instruments are operated in a way that makes the interference negligible. However, even for measurements prior to 2011, atmospheric HO₂/RO₂ ratios suggest that the magnitude of an HO₂ interference likely accounts for no more than a factor of two in the difference between measured and modeled HO₂ (Cantrell et al., 2003). Removing this interference therefore improves model-measurement HO₂ agreement, but cannot fully explain model HO₂ under-predictions at high NO_x (Griffith et al., 2016; Brune et al., 2015; Tan et al., 2017).

Modeled organic peroxy radicals are also underestimated relative to measurements by up to a factor of ten (Hornbrook et al., 2011; Tan et al., 2017). Tan et al. (2017) show that this underestimation can be most prominent at high NO_x and that further increasing a source of morning RO₂ proportional to this discrepancy improves agreement between measured and modeled peroxy radicals, but consequently overpredicts HO_x species or OH reactivity. Studies in which RO₂ (and/or HO₂) are underestimated via model calculations at high NO_x have examined possible missing VOCs or additional mechanisms that could reconcile this effect, but no such VOC or mechanism has been identified (Martinez et al., 2003; Kanaya et al., 2007; Dusanter et al., 2009; Hornbrook et al., 2011; Lu et al., 2012, 2013). To date, model under-prediction of peroxy radicals (either HO₂ or RO₂, and sometimes both species) at high NO_x levels remains unresolved.

Due to the aforementioned discrepancies between measured and modeled radicals, P(O₃) calculated from measured peroxy radicals can routinely be more than double the P(O₃) calculated from modeled HO₂ or RO₂ at high NO_x, according to several field studies conducted during the past decade (Ren et al., 2003; Kanaya et al., 2008; Spencer et al., 2009; Ren et al., 2013; Brune et al., 2015; Griffith et al., 2016; Tan et al., 2017). The Measurement of Ozone Production Sensor (MOPS) directly measures P(O₃) and can help to evaluate O₃ formation calculated from chemical mechanisms via Eqs. 2-4 (Cazorla and Brune, 2010; Baier et al., 2015). However, observed P(O₃) has also shown similar discrepancies to modeled P(O₃) at high NO or NO_x. For example, in 2010 the first version of the MOPS (Cazorla et al., 2012; Ren et al., 2013) compared directly-measured O₃ production rates to both modeled P(O₃) and that calculated from measured peroxy radicals. Observed P(O₃) and P(O₃) calculated from measured radicals were approximately equal to that modeled for NO levels up to 1 ppbv, but were significantly larger for higher values of NO.

Inaccurate model $P(O_3)$ estimation can directly affect O_3 forecasts. Im et al. (2015) and Appel et al. (2007) found that CTMs can underestimate O_3 levels above 60-80 ppbv and overestimate O_3 below 30 ppbv: errors that are typically credited to emissions and chemical mechanism choice. In addition, summertime O_3 predictions were most sensitive to regional production due to increased photochemical activity rather than transport (Im et al., 2015). It has also been found in the northeastern United States, that CTMs underestimated the effects of NO_x emissions reductions on O_3 (Gilliland et al., 2008). Thus, details of the chosen chemical mechanism can greatly affect O_3 predictions and even reverse the order of O_3 production sensitivity to its precursors, decreasing confidence in models used for developing emissions reduction strategies.

$P(O_3)$ was measured in Golden, CO in summer 2014 during a field study consisting of the Deriving Information on Surface conditions from Column and VERTically-resolved observations Relevant to Air Quality (DISCOVER-AQ) field campaign and the Front Range Air Pollution and Photochemistry Experiment (FRAPPÉ). This work describes comparisons between $P(O_3)$ measured in situ by a second-generation MOPS and $P(O_3)$ modeled using both lumped and near-explicit chemical mechanisms and we investigate the possible causes for differences observed between measured and modeled $P(O_3)$.

2 Methods

2.1 MOPS measurements

A second-generation MOPS directly measures the instantaneous O_3 production rate, $P(O_3)$, with an improved chamber and airflow design. The method is briefly described here; a more technical description of the MOPS and its modifications is detailed in Baier et al. (2015). The second-generation design aims to decrease artificial chemistry induced by air-surface interactions within the chambers. The difference in O_x (defined here as $O_3 + NO_2$) is continuously sampled by two 26.9-L trapezoidal environmental chambers with airflow somewhat like a sheath flow to isolate sampled air from chamber surfaces. The sample chamber is transparent and undergoes the same O_3 photochemistry as the atmosphere, while the reference chamber is covered with a film that blocks all ultraviolet (UV) radiation of wavelengths below 400 nm, suppressing the radical chemistry essential for new O_3 production. Positioned after the chambers, a highly-efficient UV light-emitting diode photolyzes NO_2 into O_3 in air coming through separate tubing from both the sample and reference chambers. This converter cancels any differences in the NO_x PSS caused by the reference chamber film. The difference in O_x , divided by the exposure time of air in the MOPS chambers, yields the net O_3 production rate as $P(O_x)$.

The residence time is determined by adding a pulse of O_3 to the chambers and then measuring the O_3 as a function of time (Baier et al., 2015). The resulting pulse has a mean residence time of 130 ± 5 s and the time at which the signal recedes into the background is 345 s. Thus, the exposure time of molecules in the chambers is taken to be 130 s.

The MOPS absolute uncertainty (1σ) is ± 11 ppbv h^{-1} for 10-min measurements (Baier et al., 2015), but when averaged to one hour, this uncertainty decreases to approximately 5 ppbv h^{-1} . As previously mentioned in Baier et al. (2015), the MOPS technique can produce artificial negative O_3 production rates that are roughly correlated with temperature, relative humidity, or actinic flux. As discussed in Cazorla et al. (2012), negative $P(O_3)$ rates are unrealistic during the day when OH production is large enough to sustain new NO_2 and subsequent O_3 formation from VOC oxidation.

MOPS chamber loss tests and flow visualizations have been conducted to address these artifacts. Laboratory testing indicates that wall loss of O_x and radical species is minimal (Cazorla and Brune, 2010; Baier et al., 2015). On the other hand, previous studies have found that commercial O_3 analyzers can exhibit both positive and negative responses to changes in relative humidity due to increases or decreases in water vapor (US EPA, 1999; Wilson and Birks, 2006). Additional laboratory testing
5 has been conducted to investigate the sensitivity of the MOPS Thermo Scientific O_3 analyzer used in this study. Although differences in temperature between sample and reference chamber did not play a large role in initiating baseline drifting, the MOPS O_3 analyzer exhibits a large baseline shift greater than approximately 2 ppbv when the ambient relative humidity is greater than 70%.

The MOPS precision is typically 5 ppbv h^{-1} (1σ) for one-hour averages, but O_3 analyzer drifting can degrade this precision.
10 We quantify the MOPS diurnal O_3 analyzer drift and provide a correction to the raw $P(O_3)$ data through zeroing of the MOPS chambers, either by removing the reference chamber film for an entire day, or by measuring $P(O_3)$ on cooler, cloudy days when O_3 formation is likely low (Baier et al., 2015). On these occasions, the negative O_3 differential due to high relative humidity is apparent. Since the same O_3 formation will occur in both chambers on zero days, this method retrieves a baseline $P(O_3)$ time series that can be subtracted off of the MOPS raw data. Four zeros were applied to the raw $P(O_3)$ data during this study for
15 an entire 24-hour period, with two using low O_3 production days as zeros. Positive deviations in the MOPS raw $P(O_3)$ from this negative baseline are evident during the morning hours, therefore this method extracts the positive $P(O_3)$ deviations from background O_3 analyzer drift during O_3 production hours of the day. Zeros that were taken only on days with diurnal patterns and absolute values of relative humidity that are similar to most MOPS measurements days were used in this analysis. The average zero correction that is subtracted from the raw $P(O_3)$ measurements to derive a corrected MOPS $P(O_3)$ is shown in Fig.
20 S1. In addition, we have restricted our analysis to days when the ambient relative humidity was below 70% and have tested the robustness of this threshold using a wide range of relative humidities from 70%-90% to ensure that our corrected $P(O_3)$ values were not sensitive to this threshold choice (Fig. S2).

The MOPS chamber "sheath" airflow inhibits air that has contacted the walls from being sampled in the center of the chamber exit (Baier et al., 2015). Air is then sampled from a center flow that is isolated from the chamber walls. Smoke visualizations of
25 the chamber flow, along with laboratory and atmospheric observations of chamber O_x losses less than or equal to 5%, suggest that off-gassing of O_x or other species from the MOPS chamber walls is inhibited and thus likely plays a negligible role in larger measured-than-modeled $P(O_3)$. From the laboratory and chamber testing to date, insignificant amounts of NO are lost in the MOPS chambers (Cazorla and Brune, 2010; Baier et al., 2015).

It is known that NO_2 adsorption onto the chamber walls can result in the heterogeneous formation of nitrous acid (HONO)
30 through the reaction of NO_2 with water vapor adsorbed onto surfaces (Finlayson-Pitts et al., 2003); a photolytic HONO source has also been previously reported (Rohrer et al., 2005; George et al., 2005; Stemmler et al., 2006; Langridge et al., 2009; Lee et al., 2016; Crilley et al., 2016). During the 2013 DISCOVER-AQ study in Houston, TX, excess HONO of up to five times ambient values was measured in the MOPS chambers, which can thus create excess OH and positively bias the MOPS $P(O_3)$. Although a production mechanism has not been identified, this bias was found to be a) largest between 1000-1400 LT when
35 NO_x values are high, and b) correlated with relative humidity, temperature, and J_{NO_2} (Baier et al., 2015). The MOPS inlet

is one area that is suspected to facilitate HONO production due to inevitable surface interactions with sample air entering the chambers, and we have since decreased this bias by approximately 30% through shielding the MOPS inlet face and suppressing additional HONO production. Chamber HONO values measured in Houston, TX were applied to this Golden, CO study by scaling the observed chamber HONO by the ambient NO_x ; then the possible $\text{P}(\text{O}_3)$ interference due to chamber HONO was
5 determined.

2.2 Site description and ancillary measurements

Second-generation MOPS measurements were recorded for 19 days in Golden, CO ($39^\circ 44.623' \text{N}$, $105^\circ 10.679' \text{W}$), which is located approximately 25 km west of the Denver metropolitan area. Commerce City, which houses several oil refineries, is located 30 km to the northeast. The Golden measurement site lies east of the Front Range, atop the South Table Mountain
10 mesa (1833 m asl) and amidst grass-covered terrain. The Colorado summertime climate is hot and arid with intense solar radiation. These meteorological conditions can be conducive for high O_3 formation from both local and advected precursor emissions. Ozone production can also be affected by diurnally varying, thermally driven winds; morning heating of mountains invokes easterly upslope flow, transporting precursors from Denver and the urban corridor of the Front Range westward, while downsloping afternoon westerlies can re-circulate these pollutants eastward to lower elevations (Banta, 1984).

15 Measurements used to constrain the models in this study were obtained on ground-based and aircraft platforms during DISCOVER-AQ and FRAPPÉ. Both studies were co-located in the Colorado Front Range between 17 July and 10 August 2014. Continuous, ground-based 1-min measurements of meteorological parameters and inorganic chemical species include temperature, pressure, and relative humidity, O_3 , sulfur dioxide, and NO_x . In the absence of continuous ground-based VOC measurements, C_2 - C_{10} non-methane hydrocarbons (NMHC) and organic nitrates were measured from 72 total whole-air can-
20 ister (WAC) samples that were collected in Golden and analyzed by gas chromatography (GC) and gas chromatography-mass spectrometry (GC-MS) in the laboratory. An average of five samples were taken daily over 16 days. Approximately 64% of whole air sampling occurred between 0700 and 1200 local time (LT) to capture VOC mixing ratios during morning O_3 production hours, with sparser sampling in the afternoon between 1400 and 1800 LT to examine advection from sources east of Golden, CO such as the Denver metropolitan and Commerce City regions. Median diurnal values of VOCs were constructed
25 from these point measurements to provide constraints for the model calculations. We initialized backward Hybrid Single-Particle Lagrangian Integrated Trajectory (HYSPLIT) models at 300 and 500 m heights beginning at 1600 LT and run for 12 hours using North American Model (NAM) meteorological data to determine whether the airflow in Golden could have originated from these eastern regions (Stein et al., 2015; Rolph, 2016). In general, higher NO_x and anthropogenic VOC mixing ratios were measured when HYSPLIT indicated flow from these eastern pollution sources. Thus, for days when measurements
30 were made in these plumes, separate median diurnal VOC values were constructed to more accurately represent the VOC speciation observed in Golden.

Canister VOCs were supplemented by boundary layer inorganic and organic chemical species measurements obtained on the NASA P-3B and NSF/NCAR C-130 aircraft and constant, median values were calculated for the limited times of the day when these aircraft were in the vicinity of Golden and used in the model (Table 1, Table S1). Aircraft measurements for Golden were

available after 0900 LT on P-3B overflights which occurred up to three times daily, while C-130 measurements were available after 1000 LT when this aircraft was within roughly 20 km of the measurement site. Airborne measurements of inorganic and organic species agree to within 30% on average. More information on the DISCOVER-AQ and FRAPPÈ campaigns, aircraft and ground-based platforms, and measurement methods can be found at <http://www-air.larc.nasa.gov/missions/discover-aq/discover-aq.html> and <https://www2.acom.ucar.edu/frappe>.

2.3 Model description

Two types of chemical mechanisms were used in zero-dimensional photochemical box models to calculate $P(O_3)$ for the DISCOVER-AQ and FRAPPÈ campaign period. We used the lumped Regional Atmospheric Chemistry Mechanism version 2 (RACM2) (Stockwell et al., 1997; Goliff et al., 2013), and the near-explicit Master Chemical Mechanism version 3.3.1 (MCMv331) (Jenkin et al., 2003; Bloss et al., 2005; Jenkin et al., 2015). An exhaustive list of model constraints is displayed in Table 1. Cloud-free photolysis rates were calculated using the Tropospheric Ultraviolet (TUV) model (Madronich and Flocke, 1999) for Golden, CO. These photolysis rates were scaled to J_{NO_2} calculated from continuous pyranometer measurements (LI-COR, LI-200 series) using the relationship described in Trebs et al. (2009) and then were used to constrain the models. All model constraints were interpolated to a 10-minute time step and input into the model to calculate $P(O_3)$ for the campaign period. The system of differential equations generated from both chemical mechanisms was integrated for 24 hours to allow reactive intermediates to reach steady-state. In addition, a one-day integration time is calculated to be sufficient for radical concentrations and intermediate species to reach steady-state as a two-fold or even three-fold increase in this integration time period did not impact radical concentrations or the $P(O_3)$ results described below. Longer-lived constituents not constrained in the model were given a 24-hour lifetime to both prevent buildup of these chemical species and to roughly account for advection or dilution losses. Modeled $P(O_3)$ is largely insensitive to this loss rate. We note that although transport and entrainment processes can also influence O_3 levels, zero-dimensional model runs described here do not include these processes. Instead, we focus on net $P(O_3)$ calculated with Eqs. 2-4 using modeled output.

2.4 Model uncertainty assessment

In order to explain calculated $P(O_3)$ behavior relative to the MOPS during hours of the day when there is typically a shift from VOC- to NO_x -sensitive $P(O_3)$ regimes, we explore model sensitivity to various inorganic and organic chemical species, reaction rates, product yields, and other model parameters outlined in supplementary material. For cases in which modeled O_3 sensitivity is near the transition between VOC-sensitive and NO_x -sensitive, model $P(O_3)$ uncertainty can mask the proper designation of O_3 NO_x -VOC sensitivity (Chen and Brune (2012) and references therein). Thus, understanding the uncertainty of modeled $P(O_3)$ to model inputs and parameters defines what can be said about modeled O_3 sensitivity to VOCs and NO_x .

2.4.1 RACM2

The RACM2 model includes 119 species and 363 reactions and is run using the FACSIMILE solver (Stockwell et al., 1997; Goliff et al., 2013). An explicit isoprene chemistry scheme has replaced the original RACM2 isoprene chemistry and is highlighted in Paulot et al. (2009) and Mao et al. (2013). As this mechanism aggregates VOCs based on their functional groups and OH reactivity, the RACM2 significantly reduces the number of model inputs and parameters over more explicit mechanisms that treat VOCs and their intermediate products separately.

Model uncertainty is traditionally evaluated through sensitivity analyses in order to identify inputs (observational data) and parameters (reaction rates and product yields) that create the most variance in a model output of interest. These inputs are hereby called “influential” inputs. The RACM2 model uncertainty is assessed through the use of a global sensitivity analysis for daylight hours between 0600 and 1800 LT.

A Random Sampling-High Dimensional Model Representation (RS-HDMR) analysis was performed, which varies hundreds of model constraints with relatively low computational expense (Rabitz and Alis, 1999; Li et al., 2006, 2010). The variance in modeled $P(O_3)$ due to changes in influential model constraints was calculated, with the $P(O_3)$ 1σ uncertainty derived as the total $P(O_3)$ standard deviation divided by its mean from time periods evaluated between 0600 and 1800 LT. The RS-HDMR technique used for the RACM2 model runs is detailed in Chen and Brune (2012) and Chen et al. (2012). An overview of model input uncertainties and a description of this global sensitivity analysis are presented in supplementary documentation.

2.4.2 MCMv331

The MCMv331 (Jenkin et al., 1997; Saunders et al., 2003; Bloss et al., 2005; Jenkin et al., 2015), is freely available at <http://mcm.leeds.ac.uk/MCM> and is run using a MATLAB framework described in Wolfe et al. (2016). This mechanism includes roughly 6,000 species and 17,000 reactions, treats VOCs and their intermediates separately, and uses explicit isoprene degradation chemistry described in Jenkin et al. (2015). Because of the large number of inputs in this near-explicit mechanism, the MCMv331 uncertainty was assessed through a local sensitivity approach. That is, inputs were set to their upper and lower uncertainty limits (at a 1σ confidence level) in a one-at-a-time fashion while all other constraints were held at their original values. Total MCMv331 uncertainty was calculated by adding in quadrature the upper and lower percent deviations in $P(O_3)$ due to perturbations in model constraints relative to the MCMv331 base case. Input and parameter groups that were varied to derive this uncertainty are described in supplemental documentation.

3 Results

3.1 Campaign observations and $P(O_3)$ time series

Observed and modeled $P(O_3)$ were compared between 17 July and 10 August 2014 in Golden (Fig. 1). From 17-27 July, the campaign was characterized by a warmer, drier period followed by a relatively cooler, wetter period until the end of the study. Daily O_3 mixing ratios typically peaked between 1300-1800 LT with a median value of 59 ppbv. Higher O_3 levels exceeding

80 ppbv were observed on 22, 28, and 29 July as well as 3 August. The highest O₃ levels were observed on 22 July with a maximum mixing ratio of approximately 90 ppbv.

Due to the terrain of the Front Range, the average diel wind direction during the campaign period was westerly before 0900 LT, easterly to northeasterly from 0900 to 1400 LT, and then westerly again after 1400 LT, with diel-averaged speeds ranging
5 between 2-3.5 m s⁻¹. Thus, it is possible for P(O₃) in Golden to be influenced by pollutants advected from nearby eastern source regions during the mid-morning to early afternoon.

The corrected MOPS P(O₃) maxima were routinely higher than 10 ppbv h⁻¹ on most measurement days, with diurnal peaks between 0900-1100 LT. Observed P(O₃) maxima on individual days range from 10 ppbv h⁻¹ to almost 30 ppbv h⁻¹ (Fig. 1). As mentioned earlier, MOPS P(O₃) measurements were restricted to days when the ambient relative humidity is less than 70%
10 when we have confidence that the O₃ analyzer was not affected by significant baseline drifting. This data filtering reduced the MOPS baseline variations to between -5 and 5 ppbv h⁻¹ at a 1-hour time resolution.

3.2 Modeled P(O₃) time series and comparisons to measurements

Full-campaign modeled P(O₃) is also shown in Fig. 1 for both RACM2 and MCMv331. Modeled P(O₃) for both mechanisms are a broad peak with maxima that occurred between 0900-1200 LT with values generally 10 ppbv h⁻¹ or lower. The modeled
15 P(O₃) behavior is essentially identical on a day-to-day basis for both the RACM2 and MCMv331. On several individual days, the MOPS P(O₃) measurements exhibited maxima that were a factor of two to three times higher than modeled P(O₃) values during the morning between 0900-1100 LT.

Median diel variations of MOPS and modeled P(O₃) are shown for MOPS measurement days in Fig. 2. Median observed P(O₃) began to increase around 0800 LT, peaked at greater than 10 ppbv h⁻¹ around 1000 LT, and decreased to 5 ppbv h⁻¹
20 before falling off to zero in the evening. Median modeled P(O₃) also rose beginning at about 0800 LT but peaked at around 5 ppbv h⁻¹ between 1100 and 1200 LT, and was 3-4 ppbv h⁻¹ in the afternoon. Median observed and modeled P(O₃) are in good agreement in the afternoon as shown by overlapping errorbars, but median diel MOPS P(O₃) is generally a factor of two higher than that modeled between 0900-1100 LT when NO_x and VOC levels were high due to abundant local or advected rush hour traffic emissions. The shaded region in Fig. 2 is the range of possible measured P(O₃) values obtained using the
25 range of maximum to minimum measured zero offset values. This mid-morning difference between measured and modeled diel-averaged P(O₃) is apparent over this range of zero corrections.

Figure 3 indicates P(O₃) as a function of NO levels and time of day. Similar to Cazorla et al. (2012), both measured and modeled diel P(O₃) increased between 0600-0800 LT during morning rush hour, peaked before 1200 LT, and then decreased later in the day with decreasing NO and VOC radical abundances. Occasional secondary P(O₃) peaks were exhibited between
30 1400-1600 LT in both measured and modeled P(O₃), likely due to advection of O₃ precursors from the Denver region or increased local traffic emissions. The most striking difference is that the measured P(O₃) continues to rise as NO increases while the modeled P(O₃) decreases for NO more than 1 ppbv. The missing modeled P(O₃) appears to increase monotonically with increasing NO for NO values greater than roughly 1 ppbv (Fig. 4). The difference between measured and modeled P(O₃)

is near zero up to 1 ppbv NO and almost 15 ppbv h^{-1} at 5 ppbv NO. This unexpected increase in $\text{P}(\text{O}_3)$ with increasing NO provides a clue as to what might be causing the difference between measured and modeled $\text{P}(\text{O}_3)$.

Several reasons provide confidence in these $\text{P}(\text{O}_3)$ comparisons, which result in higher $\text{P}(\text{O}_3)$ than that modeled during the morning hours. First, median $\text{P}(\text{O}_3)$ values were used instead of the mean to compare MOPS and modeled $\text{P}(\text{O}_3)$ so as not to bias diurnal $\text{P}(\text{O}_3)$ curves high or low in the event of $\text{P}(\text{O}_3)$ anomalies. Second, observed $\text{P}(\text{O}_3)$ peak values were often much greater than the hourly MOPS 1σ uncertainty on individual days as seen in Fig.1, where differences between the MOPS and modeled $\text{P}(\text{O}_3)$ were typically between 10-20 ppbv h^{-1} . Third, when different relative humidity thresholds are used to correct the raw $\text{P}(\text{O}_3)$ data, measured $\text{P}(\text{O}_3)$ consistently exhibits the same diurnal behavior with a positive deviation from modeled $\text{P}(\text{O}_3)$ around 1000 LT. Fourth, deviations from the O_3 differential baseline derived from zeroing methods are observed between 0900-1100 LT even before correcting the MOPS measurements. Thus, we have confidence in the positive MOPS $\text{P}(\text{O}_3)$ signatures, which are greater than the modeled $\text{P}(\text{O}_3)$ during the morning hours. All of these results provide confidence in the robustness of the MOPS behavior relative to the models in Figs. 1 and 2 and in the subsequent analyses.

3.3 Possible causes of the model-measurement $\text{P}(\text{O}_3)$ discrepancies

Higher morning $\text{P}(\text{O}_3)$ calculated from measured peroxy radicals has been observed at high NO with a variety of measurement methods. The MOPS observations, independent of these studies, yield similar results for the dependence of $\text{P}(\text{O}_3)$ on NO indicating that either all of these measurement methods contain similar artifacts, or that model-measurement disagreement occurs due to differences in the chemistry between observational and computational methods used to determine O_3 production rates.

We explore several hypotheses for model-measurement disagreement during the morning hours in the following sections. Possible explanations include MOPS chamber artifacts, model input and parameter uncertainties, model peroxy radical chemistry, modeled ambient HONO sources, and reactive chlorine chemistry.

3.3.1 MOPS chamber artifacts

One hypothesis is that the MOPS $\text{P}(\text{O}_3)$ is positively biased due to environmental chamber chemistry artifacts: that is, off-gassing of NO_2 , HONO, or other chemical species from the chamber walls. At higher relative humidity, chemical species adsorption onto these environmental chamber walls can be higher (Wainman et al., 2001). It is possible that subsequent desorption of NO_2 or chemical species from the walls can induce artificial chemistry in the MOPS chambers. However, as described earlier, the MOPS chamber airflow isolates sampled air from the walls of the MOPS chambers where surface reactions are most likely to occur. Chamber air closest to the walls is exhausted, leaving mostly center flow to be sampled by the MOPS O_3 analyzer.

Additionally, adsorbed NO_2 can result in heterogeneous formation of nitrous acid (HONO), and a HONO source within the chambers may result in excess $\text{P}(\text{O}_3)$ from artificial OH production (Baier et al., 2015). For the Golden, CO study, NO_x levels were a factor of three lower on average than in Houston, TX, the relative humidity was 35% lower on average, and the actinic flux was similar. Therefore, we have applied the observed chamber HONO: NO_x ratio in Houston, TX to the Golden, CO study

because the HONO production should depend linearly on NO_x adhering to the walls. We have calculated a maximum diurnal bias of +3 ppbv h^{-1} at 1000 LT (2σ) that decreases later in the day to less than 1 ppbv h^{-1} as NO_x decreases. However, this calculated bias is rather conservative; the chamber residence time of 130 s and the HONO photolysis frequency for Golden, CO can be used to determine the percentage of chamber HONO that would be converted into O_3 -producing radicals. In doing
5 so, less than 15% of chamber HONO is photolyzed. Thus, the bias for Golden, CO would be less than 0.5 ppbv h^{-1} and would contribute insignificantly to the observed $\text{P}(\text{O}_3)$ signal. In order to explain observed and modeled $\text{P}(\text{O}_3)$ differences at Golden by chamber-produced HONO, levels would need to be more than an order of magnitude larger. Therefore, the likelihood of chamber-induced $\text{P}(\text{O}_3)$ from excess HONO production causing differences between observed and modeled $\text{P}(\text{O}_3)$ is small.

3.3.2 Model input and parameter uncertainty

10 A second hypothesis is that the uncertainties in the model $\text{P}(\text{O}_3)$ are large enough that the differences in the measured and modeled $\text{P}(\text{O}_3)$ are not statistically different. Model $\text{P}(\text{O}_3)$ uncertainty has been found to be 2-5% larger during the morning hours when differences between measured and modeled $\text{P}(\text{O}_3)$ were observed. As described earlier, the RACM2 inputs and parameters affecting model $\text{P}(\text{O}_3)$ uncertainty are determined based on a RS-HDMR sensitivity analysis. Model uncertainty between 0600 and 1800 LT is similar between both chemical mechanisms (Table S4); the average modeled $\text{P}(\text{O}_3)$ uncertainty
15 (1σ) from RACM2 and MCMv331 about 30% all day. Due to similar model behavior and diurnal uncertainty estimates between the RACM2 and the MCMv331, we expect that the influential inputs between the two mechanisms – model constraints and parameters contributing largely to calculated $\text{P}(\text{O}_3)$ uncertainty – will also be similar.

Model influential inputs are specific to both location and available measurements. However, many constraints that contributed to $\text{P}(\text{O}_3)$ uncertainty in Golden, CO were found to be similar to prior sensitivity analyses of chemical mechanisms
20 conducted in much different environments (Chen and Brune (2012) and references therein). For example, two parameters consistently identified as having high importance for daytime $\text{P}(\text{O}_3)$ uncertainty involve the reaction rates, $k_{\text{OH}+\text{NO}_2}$ and $k_{\text{HO}_2+\text{NO}}$, which dictate HO_x - NO_x cycling and the production and loss of HO_x . These reaction rate coefficients have large contributions to the overall model uncertainty despite their relatively low uncertainty factors of 1.3 and 1.15 respectively (Sander et al., 2011).

25 Other model constraints influential in dictating model $\text{P}(\text{O}_3)$ uncertainty such as reaction rates, product yields and mixing ratios of species were more specific to time of day. Similar to overall results in Chen and Brune (2012), and in addition to HO_x - NO_x reaction rates, early morning $\text{P}(\text{O}_3)$ uncertainty was attributed to reaction rates involving the oxidation of reactive VOCs such as aldehydes and xylenes that initiate O_3 formation propagation and produce HO_x . Additional Golden influential reaction rates involved the decomposition and formation rates of peroxyacyl nitrates (PAN), a NO_x reservoir. As O_3 increases
30 in the afternoon, additional rates and product yields of reactions involving O_3 loss also become important, along with those between NO and other organic peroxy species (RO_2) that continue O_3 formation.

As expected, model inputs and parameters involving the formation of RO_2 or new NO_2 outside of the NO_x PSS that further propagate the O_3 formation cycle, along with inputs and parameters involving production of HO_x species, are all factors influencing model $\text{P}(\text{O}_3)$ uncertainty. Although model uncertainty is not large enough to explain model $\text{P}(\text{O}_3)$ behavior relative

to the MOPS, greater emphasis should be placed on quantifying the uncertainty in HO_x-NO_x cycling reaction rates to reduce model P(O₃) uncertainty and improve morning agreement between observed and modeled P(O₃) in Figs. 1 and 2.

3.3.3 Model peroxy radical chemistry

One hypothesis for lower modeled P(O₃) in the early morning is that modeled HO₂ is underestimated at high NO. Indeed, in
5 previous studies, measured HO₂ often exceeds modeled HO₂ for NO greater than about 1 ppbv (Faloona et al., 2000; Martinez
et al., 2003; Ren et al., 2003; Shirley et al., 2006; Emmerson et al., 2007; Kanaya et al., 2007; Dusanter et al., 2009; Sheehy
et al., 2010; Chen et al., 2010; Ren et al., 2013; Brune et al., 2015). Campaign median NO mixing ratios typically peaked
between 0900-1100 LT at about 2 ppbv with maxima as high as 7 ppbv. The largest differences in measured and modeled
P(O₃) occur during this time period when NO is greater than 1 ppbv. Thus, it is possible that the difference between measured
10 and modeled HO₂ is related to the difference between measured and modeled P(O₃).

Measurements of HO₂ and RO₂ (35% accuracy, 2σ) and OH (45% accuracy, 2σ) were made on board the NSF/NCAR
C-130 using chemical ionization mass spectrometry (CIMS) (Mauldin et al., 2003; Hornbrook et al., 2011). Figure 5 indicates
that the CIMS HO₂/OH ratio is approximately equal to the modeled HO₂/OH ratio for NO less than 1 ppbv but surpasses
modeled HO₂/OH for NO greater than 1 ppbv, declining less rapidly than models for increasing NO mixing ratios. In previous
15 studies, the agreement between measured and modeled OH has been independent of NO, so that the deviation between the
measured and modeled HO₂/OH ratio is due to deviations between measured and modeled HO₂ (Shirley et al., 2006; Kanaya
et al., 2007; Dusanter et al., 2009; Sheehy et al., 2010; Ren et al., 2013; Czader et al., 2013; Brune et al., 2015). Modeled RO₂
relative to the CIMS observed RO₂ is also underestimated at high NO (Fig. 5). Because the C-130 aircraft and ground-based
inorganic and organic species mixing ratios in Golden are within 30% on average, a disagreement between measured and
20 modeled peroxy radicals at high NO observed on the aircraft is relevant to understanding the MOPS measurements made at the
Golden ground-based site.

A hypothesis is that a missing HO₂ or RO₂ source linearly scalable to NO that was not included in the models is plausible.
However, forty-two total C₂-C₁₀ VOCs were measured by whole-air canister samples representing a large suite of organic
chemical species within the models including ones with high OH reactivities that are particularly important for O₃ formation.
25 Although measurements of VOC reactivity were not available during the field campaign time period and thus are unavailable
for comparison to modeled VOC reactivity, the suite of VOCs measured in Golden should sufficiently capture the average VOC
reactivity dependence on NO in the mechanisms used here.

If a VOC source co-emitted with NO_x is missing in the models, it would have to provide an additional HO₂ source of approxi-
mately 3x10⁷ radicals cm⁻³s⁻¹, derived from the average difference between median diel modeled and measured P(O₃). Such a
30 VOC source was investigated by adding a) an additional RO₂ source proportional to NO_x, and also b) a generic reaction involv-
ing RO₂ and NO to form HO₂ + NO₂ + RO in the MCMv331 using a bimolecular rate coefficient of 8x10⁻¹²cm³molec⁻¹s⁻¹.
In both cases, since the reaction between the methylperoxy radical (CH₃O₂) and NO is the dominant organic peroxy radical
reacting with NO to form new O₃ in both chemical mechanisms, this chemical species was used as a proxy for RO₂ in the
following case studies.

Adding this $\text{RO}_2 + \text{NO}$ reaction to form HO_2 and NO_2 in the MCMv331 only elevates modeled $\text{P}(\text{O}_3)$ throughout the day, and does not alter the diurnal $\text{P}(\text{O}_3)$ pattern (Fig. 6). Adding RO_2 in the MCMv331 proportional to NO_x improves model-measurement $\text{P}(\text{O}_3)$ agreement in the morning, but underestimates the MOPS afternoon $\text{P}(\text{O}_3)$ signal by a factor of two. The model-measurement RO_2 agreement is improved with this case study, yet HO_2/OH is still underestimated relative to
5 measurements for high NO (Fig. 5) suggesting that a missing HO_x source still remains.

Similarly, a VOC source that could explain prior model-measurement HO_x disagreement has not been identified in other literature studies where missing HO_2 was of similar magnitude to this study, even when proposed VOCs were added to model base case scenarios (Martinez et al., 2003; Kanaya et al., 2007; Dusanter et al., 2009). Brune et al. (2015) discuss that, if this missing HO_x source is also a missing OH loss, then this loss would be evidenced in measurements of OH reactivity at high
10 NO, yet no such OH loss was observed. Further, Spencer et al. (2009) found that measured peroxyntic acid (HO_2NO_2) is also elevated compared to models at high NO or NO_x . Peroxyntic acid thermally decomposes to form HO_2 and NO_2 , and can also be weakly photolyzed to form HO_2 . Kanaya et al. (2007) propose that increasing the thermal decomposition rate of HO_2NO_2 could resolve model underestimation of HO_2 at high NO, but even when this decomposition rate was increased by a factor of five, it did not correct for higher measured than modeled $\text{P}(\text{O}_3)$ at high NO. Model sensitivity runs for Golden, CO using this
15 increased decomposition rate for HO_2NO_2 in MCMv331 corroborate this same result (Fig. 6).

3.3.4 Modeled ambient HONO sources

Another hypothesis is that ambient HONO is missing from the model. The production and subsequent photolysis of nitrous acid (HONO) is an important morning HO_x source at high NO or NO_x , often comparable to or larger than other HO_x sources such as peroxide and organic VOC photolysis or O_3 photolysis followed by the subsequent reaction between $\text{O}(^1\text{D})$ and water
20 vapor to produce OH. In previous field studies, HONO photolysis was a substantial contributor to daytime HO_x production, but can be largely underpredicted by models, especially in urban environments and may be a more viable solution to the model-measurement discrepancy found in this study.

Nitrous acid was not measured during DISCOVER-AQ or FRAPPÉ, but was predicted by the gas-phase RACM2 and MCMv331 based on continuous, ground-based NO_x observations. Model HONO sources in this study only include those
25 in the gas phase. Photolytic conversion of NO_2 to HONO on aerosol surfaces (Kleffmann et al., 1998; Arens et al., 2001; Monge et al., 2010); adsorption of HNO_3 on ground surfaces and subsequent photolysis (Zhou et al., 2003, 2011) and other photolytic heterogeneous sources are not included. Therefore, model under-prediction of HONO mixing ratios in the morning can be one cause for modeled versus measured HO_2/OH disagreement.

Lee et al. (2016) indicate that, even after additional gas-phase and heterogeneous HONO sources were added to MCMv331,
30 HONO was still underestimated relative to models on average, and that a missing HONO source was correlated with J_{NO_2} , NO_2 , and the product of NO_2 and OH reactivity for an urban area. Furthermore, only model results using measured HONO were able to replicate observed OH levels (Lee et al., 2016). Field studies in which HONO was continuously measured and used to constrain both zero-dimensional and three-dimensional chemical models have been able to replicate observed OH within uncertainty levels, but still exhibit the same behavior of higher measured-than-modeled HO_2 to OH ratios and $\text{P}(\text{O}_3)$ at

high NO (Ren et al., 2003; Martinez et al., 2003; Dusanter et al., 2009; Chen et al., 2010; Czader et al., 2013; Ren et al., 2013; Brune et al., 2015).

A HONO source proportional to NO_x was added to the MCMv331, resulting in average HONO levels of 0.5-0.9 ppbv between 0700 and 1200 LT, with peak HONO levels of 0.9 ppbv at 1000 LT when MOPS $\text{P}(\text{O}_3)$ exhibits its diel peak. This case study approximately replicates the observed morning $\text{P}(\text{O}_3)$ (Fig. 6) and observed OH within uncertainty levels. However, while added HONO in the MCMv331 improves the agreement between observed and modeled diel $\text{P}(\text{O}_3)$, mid-morning HONO levels needed to do so are over a factor of two higher than those observed in other areas within Colorado (Brown et al., 2013; VandenBoer et al., 2013) and in environments with much higher NO_x levels (VandenBoer et al., 2015). Thus, the HO_2/OH ratio and the abnormally high HONO required to match the observed $\text{P}(\text{O}_3)$ provide evidence that at most only a part of the observed $\text{P}(\text{O}_3)$ can be explained by atmospheric HONO.

3.3.5 Reactive chlorine chemistry

Model under-representation of nitryl chloride (ClNO_2) production is another possible cause of the model underestimation of $\text{P}(\text{O}_3)$. Nitryl chloride serves as a nocturnal NO_x reservoir and, when photolyzed, can produce additional reactive chlorine (Cl) and nitrogen dioxide (NO_2). Reactive chlorine, even at low mixing ratios, has been found to serve as a major oxidant for VOCs, possibly increasing HO_2 and O_3 production in the early morning hours by as much as 30% (Finlayson-Pitts et al., 1989; Atkinson et al., 1999; Chang et al., 2002; Osthoff et al., 2008). The effects of ClNO_2 production on chlorine chemistry and VOC oxidation have been provided in the literature as one possible explanation for measured versus model-data HO_2 mismatch at higher NO (Thornton et al., 2010; Riedel et al., 2014; Xue et al., 2015).

Heterogeneous uptake of dinitrogen pentoxide (N_2O_5) on chloride-containing aerosol particles can produce nitric acid (HNO_3) and ClNO_2 in both marine and continental environments through the following reaction:



where k_{het} is the heterogeneous reaction rate coefficient dependent upon the aerosol surface area density and the N_2O_5 uptake coefficient on chloride-containing aerosols, and ϕ is the ClNO_2 product yield.

To test this hypothesis, we constrained the MCMv331 with continuous, cavity ring-down spectroscopy measurements of N_2O_5 (Brown et al., 2002) from a nearby measurement site (Boulder Atmospheric Observatory; 40.050°N, 105.010°W), and implemented a reduced chlorine chemical mechanism in the MCMv331 provided by Riedel et al. (2014). We assumed an N_2O_5 uptake coefficient of 0.02, which is within the range of coefficients calculated in prior field studies (Wagner et al., 2013; Riedel et al., 2013) and laboratory experiments (Zetzsch and Behnke, 1992; Behnke et al., 1997). To be consistent with previous studies near Golden, the aerosol surface area density was varied between 150 and 250 $\mu\text{m}^2 \text{cm}^{-3}$, and ϕ is varied between 0.05 and 0.1 (Thornton et al., 2010; Riedel et al., 2013). It is important to note that these assumptions vary largely with relative humidity and aerosol surface area and composition (Thornton and Abbatt, 2005; Bertram and Thornton, 2009;

Roberts et al., 2009; Thornton et al., 2010; Wagner et al., 2013; Riedel et al., 2013), but modeling over a range of values can provide a qualitative prediction of ClNO₂ production effects on model P(O₃) in this region. In each model case, the MCMv331 runs including ClNO₂ production and Cl-VOC chemistry resulted in average ClNO₂ mixing ratios between 0.04 and 0.13 ppbv during the early morning hours (0300-0600 LT) and a slight increase in diurnal P(O₃) values of less than 5%. Thus, although chlorine chemistry can have a large effect on P(O₃) during the winter and for marine environments, these model runs indicate that Cl chemistry does not play a large enough role in O₃ photochemistry during this summer campaign to explain the morning observed discrepancy between measured and modeled O₃ formation rates in Golden, CO.

3.4 Implications for O₃ mitigation strategies

3.4.1 NO_x-VOC sensitivity

The underestimation of model P(O₃) relative to the MOPS at high NO or NO_x can have far-reaching implications for model assessment of the dependency of P(O₃) on NO_x and VOCs. When examining model sensitivity to NO_x, levels were adjusted up or down by a factor of two and as a result, increasing NO_x levels decreases P(O₃) (as in a VOC-sensitive regime) while lowering NO_x levels acts to increase P(O₃) (Fig. 6).

The fraction of free radicals removed by NO_x, L_N/Q , has been used in the literature to assess NO_x-VOC sensitivity in regions experiencing high O₃ (Daum et al., 2004; Kleinman, 2005; Ren et al., 2013). Here, L_N is the rate of total free radical removal by NO_x, and Q is the total radical production rate. When significantly above 0.5, the atmosphere is within a VOC-sensitive regime, while when significantly below 0.5, the atmosphere is within a NO_x-sensitive regime (Kleinman, 2005). The median L_N/Q was calculated with the RACM2 using full-campaign observations, indicating that the Golden, CO modeled P(O₃) is VOC-sensitive before 1200 LT and NO_x-sensitive thereafter (Fig. S4). During DISCOVER-AQ and FRAPPÈ, model sensitivity studies conducted for the Boulder Atmospheric Observatory site just northeast of Golden also found maximum photochemical O₃ to be largely NO_x-sensitive in the afternoon (McDuffie et al., 2016). If peroxy radicals are underestimated by chemical mechanisms relative to observations for NO levels greater than a few ppbv, then the total radical production rate, Q , may also be underestimated, thereby shifting L_N/Q towards NO_x-sensitivity in the early morning and prolonging this regime during times of the day when O₃ production is largest.

The largest O₃ formation rates are measured between 0900-1100 LT when NO_x and VOC emissions are high and the mixing layer depth is relatively developed at 600 to 1000 m on average. Although a shallower mixing layer could be one reason for high MOPS P(O₃) before 1100 LT, we note that secondary diurnal MOPS P(O₃) peaks are also evidenced on individual days alongside increased NO_x and VOCs during afternoon rush hour in a fully-developed mixing layer. Further, high P(O₃) and the shift from VOC- to NO_x-sensitivity in the late morning could be attributed to early-morning entrainment of VOCs from the free troposphere in the absence of NO_x entrainment. However, these VOCs in the upper troposphere are longer-lived and are less important in propagating O₃ formation than other, higher reactivity VOCs. Therefore, although entrainment of species during the morning hours and the depth of the mixing layer influence NO_x-VOC sensitivity and these high morning P(O₃) rates, it is more likely that O₃ precursor species at the surface level are the predominant factors influencing P(O₃) for this study.

Although longer-term analyses are generally required to suggest effective O₃ reduction strategies, if the P(O₃) NO_x-VOC sensitivity is shifted more towards a NO_x-sensitive regime in the morning as the MOPS observations suggest, reducing NO_x would be an effective strategy for O₃ mitigation in Golden, CO and its immediate surroundings.

3.4.2 O_x advection

- 5 Ozone formation precursors can be transported westward to Golden because of the Colorado Front Range terrain and its induced wind patterns. When air in Golden is influenced by O₃ precursor emissions from the east (e.g. the Denver metropolitan and Commerce City regions), greater anthropogenic VOC and NO mixing ratios are measured on average. Thus, we evaluate calculated O₃ advection using Eq. (1) in an attempt to evaluate the impact of O₃ advection derived from the MOPS and the models on observed O₃ patterns in Golden.
- 10 Measured O_x maxima are 2-7 ppbv greater on these “plume” days than when air is advected from elsewhere, and higher P(O₃) is measured by the MOPS than is modeled by the RACM2 and MCMv331 (Fig. 7). This result is roughly consistent with the difference between measured and modeled P(O₃) as a function of NO shown in Fig. 4. When winds are not easterly (“non-plume” days), lower levels of anthropogenic VOCs and NO, and lower O_x maxima are observed. Average measured diel P(O₃) is also 20% lower than on plume days. The MOPS behavior stands in contrast to the models, where average diel RACM2
- 15 and MCMv331 P(O₃) is approximately 30% higher on non-plume days than on plume days.

A simple advection analysis was performed to determine the factors in Eq. (1) that most contribute to observed O_x levels in Fig. 7 for the campaign period. The transport rate of O_x out of the mixing layer through deposition is calculated to be at most 1 ppbv h⁻¹ and is neglected here. The morning O₃ entrainment rate during DISCOVER-AQ and FRAPPÈ has been calculated for the Colorado Front Range region to be 5 ppbv h⁻¹ on average, with afternoon average entrainment rates of approximately

20 -1 ppbv h⁻¹ (Kaser et al. (2016), *in prep*). Assuming an average entrainment rate of 5 ppbv h⁻¹ for morning hours between 0600-1200 LT and an O_x entrainment rate of -1 ppbv h⁻¹ for times between 1200-1800 LT and subtracting diel entrainment and observed P(O_x) from the local diel O_x rate of change, the average O_x advection rate derived from MOPS and models between 0600-1800 LT is -5.4 to -2.4 ppbv h⁻¹ on plume days, and -1.7 to -3.5 ppbv h⁻¹ for all other days, respectively. This quick calculation suggests that advection contributes weakly to observed O_x, while either entrainment or P(O_x) dominate the

25 O_x patterns observed in Golden and its surrounding areas. Because these advection rates are derived quantities from the MOPS and the models, and both methods for determining P(O_x) contain substantial uncertainty, it is difficult to quantitatively assess O_x advection rates in Golden, CO. Decreasing the uncertainty in P(O_x) is thus salient for accurately calculating the terms in Eq. (1) contributing to observed O_x levels in the Colorado Front Range.

4 Conclusions

- 30 Comparisons were made between P(O₃) measured in situ by a second-generation Penn State MOPS and photochemical box modeled P(O₃) using both lumped and near-explicit chemical mechanisms. These comparisons during the 2014 DISCOVER-AQ and FRAPPÈ field campaigns in the Colorado Front Range show that median diel modeled P(O₃) is underestimated relative

to the MOPS by roughly a factor of two in mid-morning, when actinic flux is increasing and morning rush hour abundances of NO_x and VOCs are decreasing. This result corroborates to previous studies that had $\text{P}(\text{O}_3)$ measured by MOPSS (Cazorla et al., 2012; Baier et al., 2015). Thus, this model-data $\text{P}(\text{O}_3)$ mismatch appears to come from unknowns in the chamber or atmospheric chemistry and not from one particular environment.

- 5 The uncertainties in both the measurement and the model are substantial. The measurement uncertainty is about ± 5 ppbv h^{-1} , with the largest portion due to the zeroing of the daily negative drifting of the differential O_3 measurement. Model $\text{P}(\text{O}_3)$ uncertainty is about 30% (1σ confidence) during peak $\text{P}(\text{O}_3)$ hours; factors such as uncertainty in the kinetic rate coefficients of HO_x - NO_x cycling reactions are most significant. Despite these uncertainties, the difference between the diel behavior and values of measured and modeled $\text{P}(\text{O}_3)$ is significant.
- 10 Upon further analysis of the discrepancy between measured and modeled $\text{P}(\text{O}_3)$ at high NO_x , it was found that the measured peroxy radical behavior as a function of NO was similar to studies previously reported in the literature. In these studies, the measured HO_2/OH ratio and measured RO_2 decrease less rapidly than that modeled for higher NO levels, causing measured or calculated $\text{P}(\text{O}_3)$ to be several factors larger than modeled $\text{P}(\text{O}_3)$. As such, neither MOPS chamber artifacts, reactive chlorine chemistry, nor model case studies that add additional peroxy radical sources can fully explain this model-data $\text{P}(\text{O}_3)$ mismatch.
- 15 While an additional HONO source proportional to NO_x can help to improve diel $\text{P}(\text{O}_3)$ patterns, mid-morning HONO levels needed to approximate MOPS $\text{P}(\text{O}_3)$ are at least a factor of two higher than HONO levels observed in other environments, including ones nearby in Colorado. Additional RO_2 sources can approximate $\text{P}(\text{O}_3)$ morning diurnal patterns, but underestimate $\text{P}(\text{O}_3)$ in the afternoon relative to the MOPS by roughly a factor of two. Neither peroxy radical addition mechanism can approximate the behavior of HO_x radicals as a function of NO relative to measurements.
- 20 More research must be conducted to understand the differences between modeled and measured $\text{P}(\text{O}_3)$. The second-generation MOPS is still in early stages of development and more rigorous testing is needed to decrease the MOPS absolute measurement uncertainty through the reduction of O_3 analyzer drifting and improvement in the precision of this analyzer. Conversely, model comparisons highlight the need to revisit current mechanism chemistry, including possible missing peroxy radical chemistry at high NO_x levels.
- 25 If the MOPS accurately predicts morning $\text{P}(\text{O}_3)$, then L_N/Q metrics from observation-constrained models that calculate radical mixing ratios may be incorrectly assessing NO_x or VOC O_3 production sensitivity and the efficacy of O_3 reduction strategies. The use of these mechanisms in CTMs could create significant differences between modeled and observed $\text{P}(\text{O}_3)$ during peak O_3 production hours. Further, the plethora of chemical mechanisms available for use in these models create a large spread in model O_3 predictions. Thus, differences between measured and modeled $\text{P}(\text{O}_3)$ can have substantial and
- 30 potentially costly implications for O_3 mitigation strategies that are put in place in O_3 NAAQS non-attainment areas. The MOPS measurements indicate that $\text{P}(\text{O}_3)$ in Golden, CO and its surrounding areas is more NO_x -sensitive than models currently predict in the morning hours, suggesting that NO_x emission reductions in this region could be a viable solution for O_3 mitigation.

5 Data availability

The MCM version 3.3.1 is freely available at <http://mcm.leeds.ac.uk/MCM/> and the University of Washington Chemical Model (UWCM) framework used to run MCMv331 is available to the public from G. Wolfe. Meteorological and chemical data collected during the DISCOVER-AQ and FRAPPÈ studies are available at <http://www-air.larc.nasa.gov/missions/discover-aq/discover-aq.html> and <https://www2.acom.ucar.edu/frappe>.

Author S. Brown serves on the editorial board of this journal. No other authors declare any conflicts of interest.

Acknowledgements. We gratefully acknowledge the entire DISCOVER-AQ and FRAPPÈ teams for the collection of ground and airborne measurement data in this work. We kindly acknowledge R. Cohen for the provision of data used in these model studies. PTR-ToF-MS measurements during DISCOVER-AQ were carried out by P. Eichler, T. Mikoviny, and M. Müller, and were supported by the Austrian Federal Ministry for Transport, Innovation and Technology (bmvit) through the Austrian Space Applications Programme (ASAP) of the Austrian Research Promotion Agency (FFG). We thank G. Wolfe for provision of and help with the MCM model framework, W. Goliff for the provision of the RACM2, and J. Thornton for thoughtful discussions. We thank the two anonymous reviewers for their useful comments. For the use of the web version of the HYSPLIT model (<http://www.ready.noaa.gov>), we acknowledge the NOAA Air Resources Laboratory.

This work was funded by NASA grants NNX14AR83G and NNX12AB84G.

References

- Apel, E., Hills, A., Lueb, R., Zindel, S., Eisele, S., and Riemer, D.: A fast-GC/MS system to measure C2 to C4 carbonyls and methanol aboard aircraft, *Journal of Geophysical Research: Atmospheres*, 108, 2003.
- Appel, K. W., Gilliland, A. B., Sarwar, G., and Gilliam, R. C.: Evaluation of the Community Multiscale Air Quality (CMAQ) model version 4.5: Sensitivities impacting model performance: Part I: Ozone, *Atmospheric Environment*, 41, 9603–9615, doi:10.1016/j.atmosenv.2007.08.044, <http://www.sciencedirect.com/science/article/pii/S1352231007007534>, 2007.
- Arens, F., Gutzwiller, L., Baltensperger, U., Gäggeler, H. W., and Ammann, M.: Heterogeneous reaction of NO₂ on diesel soot particles, *Environmental science & technology*, 35, 2191–2199, 2001.
- Atkinson, R., Baulch, D., Cox, R., Hampson Jr, R., Kerr, J., Rossi, M., and Troe, J.: Evaluated kinetic and photochemical data for atmospheric chemistry, organic species: Supplement VII, *Journal of Physical and chemical reference Data*, 28, 191–393, 1999.
- Baier, B. C., Brune, W. H., Lefer, B. L., Miller, D. O., and Martins, D. K.: Direct ozone production rate measurements and their use in assessing ozone source and receptor regions for Houston in 2013, *Atmospheric Environment*, 114, 83–91, doi:10.1016/j.atmosenv.2015.05.033, <http://www.sciencedirect.com/science/article/pii/S1352231015301060>, 2015.
- Banta, R. M.: Daytime Boundary-Layer Evolution over Mountainous Terrain. Part 1: Observations of the Dry Circulations, *Mon. Wea. Rev.*, 112, 340–356, doi:10.1175/1520-0493(1984)112<0340:DBLEOM>2.0.CO;2, [http://journals.ametsoc.org/doi/abs/10.1175/1520-0493\(1984\)112%3C0340%3ADBLEOM%3E2.0.CO%3B2](http://journals.ametsoc.org/doi/abs/10.1175/1520-0493(1984)112%3C0340%3ADBLEOM%3E2.0.CO%3B2), 1984.
- Behnke, W., George, C., Scheer, V., and Zetzsch, C.: Production and decay of ClNO₂ from the reaction of gaseous N₂O₅ with NaCl solution: Bulk and aerosol experiments, *J. Geophys. Res.*, 102, 3795–3804, doi:10.1029/96JD03057, <http://onlinelibrary.wiley.com/doi/10.1029/96JD03057/abstract>, 1997.
- Bell, M. L., McDermott, A., Zeger, S., Samet, J., and Dominici, F.: Ozone and Short-term Mortality in 95 US Urban Communities 1987-2000, *Journal of the American Medical Association*, 292, doi:10.1001/jama.292.19.2372, 2004.
- Bertram, T. H. and Thornton, J. A.: Toward a general parameterization of N₂O₅ reactivity on aqueous particles: the competing effects of particle liquid water, nitrate and chloride, *Atmos. Chem. Phys.*, 9, 8351–8363, doi:10.5194/acp-9-8351-2009, <http://www.atmos-chem-phys.net/9/8351/2009/>, 2009.
- Bloss, C., Wagner, V., Jenkin, M. E., Volkamer, R., Bloss, W. J., Lee, J. D., Heard, D. E., Wirtz, K., Martin-Reviejo, M., Rea, G., Wenger, J. C., and Pilling, M. J.: Development of a detailed chemical mechanism (MCMv3.1) for the atmospheric oxidation of aromatic hydrocarbons, *Atmospheric Chemistry and Physics*, 5, 641–664, doi:10.5194/acp-5-641-2005, <http://www.atmos-chem-phys.net/5/641/2005/>, 2005.
- Brown, S. S., Stark, H., Ciciora, S. J., McLaughlin, R. J., and Ravishankara, A.: Simultaneous in situ detection of atmospheric NO₃ and N₂O₅ via cavity ring-down spectroscopy, *Review of scientific instruments*, 73, 3291–3301, 2002.
- Brown, S. S., Thornton, J. A., Keene, W. C., Pszenny, A. A., Sive, B. C., Dube, W. P., Wagner, N. L., Young, C. J., Riedel, T. P., Roberts, J. M., et al.: Nitrogen, Aerosol Composition, and Halogens on a Tall Tower (NACHTT): Overview of a wintertime air chemistry field study in the front range urban corridor of Colorado, *Journal of Geophysical Research: Atmospheres*, 118, 8067–8085, 2013.
- Brune, W. H., Baier, B. C., Thomas, J., Ren, X., Cohen, R., Pusede, S. E., Browne, E., Goldstein, A., Gentner, D. R., Keutsch, F. N., Thornton, J. A., Harrold, S., Lopez-Hilfiker, F., and Wennberg, P. O.: Ozone Production Chemistry in the Presence of Urban Plumes, *Faraday Discuss.*, doi:10.1039/C5FD00204D, <http://pubs.rsc.org/en/content/articlelanding/2015/fd/c5fd00204d>, 2015.
- Calvert, J. G., Orlando, J. J., Stockwell, W. R., and Wallington, T. J.: *The Mechanisms of Reactions Influencing Atmospheric Ozone*, Oxford University Press, 2015.

- Cantrell, C. A., Edwards, G., Stephens, S., Mauldin, R., Zondlo, M., Kosciuch, E., Eisele, F., Shetter, R., Lefer, B., Hall, S., et al.: Peroxy radical behavior during the Transport and Chemical Evolution over the Pacific (TRACE-P) campaign as measured aboard the NASA P-3B aircraft, *Journal of Geophysical Research: Atmospheres*, 108, 2003.
- Cazorla, M. and Brune, W. H.: Measurement of Ozone Production Sensor, *Atmospheric Measurement Techniques*, 3, 545–555, doi:10.5194/amt-3-545-2010, 2010.
- 5 Cazorla, M., Brune, W. H., Ren, X., and Lefer, B.: Direct measurement of ozone production rates in Houston in 2009 and comparison with two estimation methods, *Atmos. Chem. Phys.*, 12, 1203–1212, doi:10.5194/acp-12-1203-2012, 2012.
- Chang, S., McDonald-Buller, E., Kimura, Y., Yarwood, G., Neece, J., Russell, M., Tanaka, P., and Allen, D.: Sensitivity of urban ozone formation to chlorine emission estimates, *Atmospheric Environment*, 36, 4991–5003, 2002.
- 10 Chen, S. and Brune, W. H.: Global sensitivity analysis of ozone production and O₃-NO_x-VOC limitation based on field data, *Atmospheric Environment*, 55, 288–296, doi:10.1016/j.atmosenv.2012.03.061, 2012.
- Chen, S., Ren, X., Mao, J., Chen, Z., Brune, W. H., Lefer, B., Rappenglück, B., Flynn, J., Olson, J., and Crawford, J. H.: A comparison of chemical mechanisms based on TRAMP-2006 field data, *Atmospheric Environment*, 44, 4116–4125, doi:10.1016/j.atmosenv.2009.05.027, 2010.
- 15 Chen, S., Brune, W. H., Oluwole, O. O., Kolb, C. E., Bacon, F., Li, G., and Rabitz, H.: Global sensitivity analysis of the regional atmospheric chemical mechanism: an application of random sampling-high dimensional model representation to urban oxidation chemistry, *Environmental science & technology*, 46, 11 162–11 170, doi:10.1021/es301565w, PMID: 22963531, 2012.
- Colman, J. J., Swanson, A. L., Meinardi, S., Sive, B. C., Blake, D. R., and Rowland, F. S.: Description of the analysis of a wide range of volatile organic compounds in whole air samples collected during PEM-Tropics A and B, *Analytical Chemistry*, 73, 3723–3731, 2001.
- 20 Crilley, L., Kramer, L., Pope, F. D., Whalley, L. K., Cryer, D. R., Heard, D. E., Lee, J., Reed, C., and Bloss, W.: On the interpretation of in situ HONO observations via photochemical steady state, *Faraday Discussions*, 2016.
- Czader, B. H., Li, X., and Rappenglueck, B.: CMAQ modeling and analysis of radicals, radical precursors, and chemical transformations, *J. Geophys. Res. Atmos.*, 118, 11,376–11,387, doi:10.1002/jgrd.50807, <http://onlinelibrary.wiley.com/doi/10.1002/jgrd.50807/abstract>, 2013.
- 25 Daum, P. H., Kleinman, L. I., Springston, S. R., Nunnermacker, L. J., Lee, Y.-N., Weinstein-Lloyd, J., Zheng, J., and Berkowitz, C. M.: Origin and properties of plumes of high ozone observed during the Texas 2000 Air Quality Study (TexAQS 2000), *J. Geophys. Res.*, 109, D17 306, doi:10.1029/2003JD004311, <http://onlinelibrary.wiley.com/doi/10.1029/2003JD004311/abstract>, 2004.
- Day, D., Wooldridge, P., Dillon, M., Thornton, J., and Cohen, R.: A thermal dissociation laser-induced fluorescence instrument for in situ detection of NO₂, peroxy nitrates, alkyl nitrates, and HNO₃, *Journal of Geophysical Research: Atmospheres*, 107, 2002.
- 30 Dodge, M. C.: Chemical oxidant mechanisms for air quality modeling: critical review, *Atmospheric Environment*, 34, 2103–2130, doi:10.1016/S1352-2310(99)00461-6, <http://www.sciencedirect.com/science/article/pii/S1352231099004616>, 2000.
- Dusanter, S., Vimal, D., Stevens, P., Volkamer, R., and Molina, L.: Measurements of OH and HO₂ concentrations during the MCMA-2006 field campaign–Part 1: Deployment of the Indiana University laser-induced fluorescence instrument, *Atmospheric Chemistry and Physics*, 9, 1665–1685, 2009.
- 35 Emmerson, K., Carslaw, N., Carpenter, L., Heard, D., Lee, J., and Pilling, M.: Urban atmospheric chemistry during the PUMA campaign 1: Comparison of modelled OH and HO₂ concentrations with measurements, *Journal of Atmospheric Chemistry*, 52, 143–164, 2005.

- Emmerson, K., Carslaw, N., Carslaw, D., Lee, J., McFiggans, G., Bloss, W., Gravestock, T., Heard, D., Hopkins, J., Ingham, T., Pilling, M. J., Smith, S., Jacob, D. J., and Monks, P. S.: Free radical modelling studies during the UK TORCH Campaign in Summer 2003, 7, 167–181, <http://www.atmos-chem-phys.org/7/167/2007/acp-7-167-2007.pdf>, 2007.
- Faloona, I., Tan, D., Brune, W. H., Jaeglé, L., Jacob, D. J., Kondo, Y., Koike, M., Chatfield, R., Pueschel, R., Ferry, G., Sachse, G., Vay, S., Anderson, B., Hannon, J., and Fuelberg, H.: Observations of HO_x and its relationship with NO_x in the upper troposphere during SONEX, *J. Geophys. Res.*, 105, 3771–3783, doi:10.1029/1999JD900914, <http://onlinelibrary.wiley.com/doi/10.1029/1999JD900914/abstract>, 2000.
- Finlayson-Pitts, B., Wingen, L., Sumner, A., Syomin, D., and Ramazan, K.: The heterogenous hydrolysis of NO₂ in laboratory systems and in outdoor and indoor atmospheres: An integrated mechanism, *Physical Chemistry Chemical Physics*, 5, 223–242, doi:10.1039/B208564J, 2003.
- 10 Finlayson-Pitts, B. J. and Pitts, J. N.: The chemical basis of air quality- Kinetics and mechanisms of photochemical air pollution and application to control strategies, *Advances in environmental science and technology.*, 7, 75–162, 1977.
- Finlayson-Pitts, B. J., Ezell, M. J., and Pitts, J. N.: Formation of chemically active chlorine compounds by reactions of atmospheric NaCl particles with gaseous N₂O₅ and ClONO₂, *Nature*, 337, 241–244, doi:10.1038/337241a0, <http://www.nature.com/nature/journal/v337/n6204/abs/337241a0.html>, 1989.
- 15 Fuchs, H., Bohn, B., Hofzumahaus, A., Holland, F., Lu, K., Nehr, S., Rohrer, F., and Wahner, A.: Detection of HO₂ by laser-induced fluorescence: calibration and interferences from RO₂ radicals, *Atmospheric Measurement Techniques*, 4, 1209, 2011.
- George, C., Strekowski, R., Kleffmann, J., Stemmler, K., and Ammann, M.: Photoenhanced uptake of gaseous NO₂ on solid organic compounds: a photochemical source of HONO, *Faraday Discussions*, 130, 195–210, 2005.
- Gilliland, A. B., Hogrefe, C., Pinder, R. W., Godowitch, J. M., Foley, K. L., and Rao, S. T.: Dynamic evaluation of regional air quality 20 models: Assessing changes in O₃ stemming from changes in emissions and meteorology, *Atmospheric Environment*, 42, 5110–5123, doi:10.1016/j.atmosenv.2008.02.018, <http://www.sciencedirect.com/science/article/pii/S1352231008001374>, 2008.
- Goliff, W. S., Stockwell, W. R., and Lawson, C. V.: The regional atmospheric chemistry mechanism, version 2, *Atmospheric Environment*, 68, 174–185, doi:10.1016/j.atmosenv.2012.11.038, <http://www.sciencedirect.com/science/article/pii/S1352231012011065>, 2013.
- Griffith, S., Hansen, R., Dusanter, S., Michoud, V., Gilman, J., Kuster, W., Veres, P., Graus, M., Gouw, J., Roberts, J., et al.: Measurements 25 of hydroxyl and hydroperoxy radicals during CalNex-LA: Model comparisons and radical budgets, *Journal of Geophysical Research: Atmospheres*, 121, 4211–4232, 2016.
- Haagen-Smit, A. J., Bradley, C. E., and Fox, M. M.: Ozone Formation in Photochemical Oxidation of Organic Substances, *Ind. Eng. Chem.*, 45, 2086–2089, doi:10.1021/ie50525a044, <http://dx.doi.org/10.1021/ie50525a044>, 1953.
- Hofzumahaus, A., Rohrer, F., Lu, K., Bohn, B., Brauers, T., Chang, C.-C., Fuchs, H., Holland, F., Kita, K., Kondo, Y., Li, X., Lou, S., Shao, 30 M., Zeng, L., Wahner, A., and Zhang, Y.: Amplified Trace Gas Removal in the Troposphere, *Science*, 324, 1702–1704, 2009.
- Hornbrook, R. S., Crawford, J. H., Edwards, G. D., Goyea, O., Mauldin III, R. L., Olson, J. S., and Cantrell, C. A.: Measurements of tropospheric HO₂ and RO₂ by oxygen dilution modulation and chemical ionization mass spectrometry, *Atmos. Meas. Tech.*, 4, 735–756, doi:10.5194/amt-4-735-2011, <http://www.atmos-meas-tech.net/4/735/2011/>, 2011.
- Im, U., Bianconi, R., Solazzo, E., Kioutsioukis, I., Badia, A., Balzarini, A., Baró, R., Bellasio, R., Brunner, D., Chemel, C., et al.: Evaluation 35 of operational on-line-coupled regional air quality models over Europe and North America in the context of AQMEII phase 2. Part I: Ozone, *Atmospheric Environment*, 115, 404–420, 2015.

- Jaegle, L., Jacob, D. J., Brune, W. H., Tan, D., Faloon, I. C., Weinheimer, A. J., Ridley, B. A., Campos, T. L., and Sachse, G. W.: Sources of HO_x and production of ozone in the upper troposphere over the United States, *Geophysical Research Letters*, 25, 1709–1712, doi:10.1029/98GL00041, <http://dx.doi.org/10.1029/98GL00041>, 1998.
- 5 Jeffries, H. E. and Tonnesen, S.: A comparison of two photochemical reaction mechanisms using mass balance and process analysis, *Atmospheric Environment*, 28, 2991–3003, 1994.
- Jenkin, M. E., Saunders, S. M., and Pilling, M. J.: The tropospheric degradation of volatile organic compounds: a protocol for mechanism development, *Atmospheric Environment*, 31, 81–104, doi:10.1016/S1352-2310(96)00105-7, <http://www.sciencedirect.com/science/article/pii/S1352231096001057>, 1997.
- Jenkin, M. E., Saunders, S. M., Wagner, V., and Pilling, M. J.: Protocol for the development of the Master Chemical Mechanism, MCM v3 (Part B): tropospheric degradation of aromatic volatile organic compounds, *Atmos. Chem. Phys.*, 3, 181–193, doi:10.5194/acp-3-181-2003, <http://www.atmos-chem-phys.net/3/181/2003/>, 2003.
- 10 Jenkin, M. E., Young, J. C., and Rickard, A. R.: The MCM v3.3.1 degradation scheme for isoprene, *Atmos. Chem. Phys.*, 15, 11 433–11 459, doi:10.5194/acp-15-11433-2015, <http://www.atmos-chem-phys.net/15/11433/2015/>, 2015.
- Jimenez, P., Baldasano, J. M., and Dabdub, D.: Comparison of photochemical mechanisms for air quality modeling, *Atmospheric Environment*, 37, 4179–4194, doi:10.1016/S1352-2310(03)00567-3, 2003.
- 15 Kanaya, Y., Cao, R., Akimoto, H., Fukuda, M., Komazaki, Y., Yokouchi, Y., Koike, M., Tanimoto, H., Takegawa, N., and Kondo, Y.: Urban photochemistry in central Tokyo: 1. Observed and modeled OH and HO₂ radical concentrations during the winter and summer of 2004, *J. Geophys. Res.*, 112, D21 312, doi:10.1029/2007JD008670, <http://onlinelibrary.wiley.com/doi/10.1029/2007JD008670/abstract>, 2007.
- Kanaya, Y., Fukuda, M., Akimoto, H., Takegawa, N., Komazaki, Y., Yokouchi, Y., Koike, M., and Kondo, Y.: Urban photochemistry in central Tokyo: 2. Rates and regimes of oxidant (O₃+ NO₂) production, *Journal of Geophysical Research: Atmospheres*, 113, 2008.
- 20 Kaser, L., Patton, E., Pfister, G. G., Weinheimer, A., and Coauthors: The effect of vertical mixing on observed and modeled surface ozone in the Colorado Front Range, *in prep*, 2016.
- Kleffmann, J., Becker, K., and Wiesen, P.: Heterogeneous NO₂ conversion processes on acid surfaces: possible atmospheric implications, *Atmospheric Environment*, 32, 2721–2729, 1998.
- 25 Kleinman, L. I.: The dependence of tropospheric ozone production rate on ozone precursors, *Atmospheric Environment*, 39, 575–586, doi:10.1016/j.atmosenv.2004.08.047, 2005.
- Kleinman, L. I., Daum, P. H., Lee, J. H., Lee, Y.-N., Nunnermacker, L. J., Springston, S. R., Newman, L., Weinstein-Lloyd, J., and Sillman, S.: Dependence of ozone production on NO and hydrocarbons in the troposphere, *Geophysical Research Letters*, 24, 2299–2302, doi:10.1029/97GL02279, 1997.
- 30 Krupa, S. V. and Manning, W. J.: Toxic Substance in the Environment Atmospheric ozone: Formation and effects on vegetation, *Environmental Pollution*, 50, 101–137, doi:10.1016/0269-7491(88)90187-X, <http://www.sciencedirect.com/science/article/pii/026974918890187X>, 1988.
- Kuhn, M., Builtjes, P. J. H., Poppe, D., Simpson, D., Stockwell, W. R., Andersson-Sköld, Y., Baart, A., Das, M., Fiedler, F., Hov, , Kirchner, F., Makar, P. A., Milford, J. B., Roemer, M. G. M., Ruhnke, R., Strand, A., Vogel, B., and Vogel, H.: Intercomparison of the gas-phase chemistry in several chemistry and transport models, *Atmospheric Environment*, 32, 693–709, doi:10.1016/S1352-2310(97)00329-4, <http://www.sciencedirect.com/science/article/pii/S1352231097003294>, 1998.
- 35

- Langridge, J. M., Gustafsson, R. J., Griffiths, P. T., Cox, R. A., Lambert, R. M., and Jones, R. L.: Solar driven nitrous acid formation on building material surfaces containing titanium dioxide: A concern for air quality in urban areas?, *Atmospheric Environment*, 43, 5128–5131, 2009.
- Lee, J., Whalley, L., Heard, D., Stone, D., Dunmore, R., Hamilton, J., Young, D., Allan, J., Laufs, S., and Kleffmann, J.: Detailed budget analysis of HONO in central London reveals a missing daytime source, *Atmospheric Chemistry and Physics*, 16, 2747–2764, 2016.
- Li, G., Hu, J., Wang, S.-W., Georgopoulos, P. G., Schoendorf, J., and Rabitz, H.: Random Sampling-High Dimensional Model Representation (RS-HDMR) and Orthogonality of Its Different Order Component Functions, *J. Phys. Chem. A*, 110, 2474–2485, doi:10.1021/jp054148m, <http://dx.doi.org/10.1021/jp054148m>, 2006.
- Li, G., Rabitz, H., Yelvington, P. E., Oluwole, O. O., Bacon, F., Kolb, C. E., and Schoendorf, J.: Global Sensitivity Analysis for Systems with Independent and/or Correlated Inputs, *J. Phys. Chem. A*, 114, 6022–6032, doi:10.1021/jp9096919, <http://dx.doi.org/10.1021/jp9096919>, 2010.
- Lu, K., Rohrer, F., Holland, F., Fuchs, H., Bohn, B., Brauers, T., Chang, C., Häsel, R., Hu, M., Kita, K., et al.: Observation and modelling of OH and HO₂ concentrations in the Pearl River Delta 2006: a missing OH source in a VOC rich atmosphere, *Atmospheric chemistry and physics*, 12, 1541–1569, 2012.
- Lu, K., Hofzumahaus, A., Holland, F., Bohn, B., Brauers, T., Fuchs, H., Hu, M., Häsel, R., Kita, K., Kondo, Y., et al.: Missing OH source in a suburban environment near Beijing: observed and modelled OH and HO₂ concentrations in summer 2006, *Atmospheric Chemistry and Physics*, 13, 1057–1080, 2013.
- Luecken, D., Phillips, S., Sarwar, G., and Jang, C.: Effects of using the CB05 vs. SAPRC99 vs. CB4 chemical mechanism on model predictions: Ozone and gas-phase photochemical precursor concentrations, *Atmospheric Environment*, 42, 5805–5820, doi:10.1016/j.atmosenv.2007.08.056, <http://www.sciencedirect.com/science/article/pii/S1352231007007728>, 2008.
- Luecken, D. J., Tonnesen, G. S., and Sickles, J. E., I.: Differences in NO_y speciation predicted by three photochemical mechanisms, *Atmospheric Environment*, 33, 1073–1084, doi:10.1016/S1352-2310(98)00319-7, <http://www.sciencedirect.com/science/article/pii/S1352231098003197>, 1999.
- Madronich, S. and Flocke, S.: The Role of Solar Radiation in Atmospheric Chemistry, in: *Environmental Photochemistry*, edited by Boule, D. P., no. 2 / 2L in *The Handbook of Environmental Chemistry*, pp. 1–26, Springer Berlin Heidelberg, http://link.springer.com/chapter/10.1007/978-3-540-69044-3_1, 1999.
- Mao, J., Paulot, F., Jacob, D. J., Cohen, R. C., Crouse, J. D., Wennberg, P. O., Keller, C. A., Hudman, R. C., Barkley, M. P., and Horowitz, L. W.: Ozone and organic nitrates over the eastern United States: Sensitivity to isoprene chemistry, *Journal of Geophysical Research: Atmospheres*, 118, 2013.
- Martinez, M., Harder, H., Kovacs, T. A., Simpas, J. B., Bassis, J., Leshner, R., Brune, W. H., Frost, G. J., Williams, E. J., Stroud, C. A., Jobson, B. T., Roberts, J. M., Hall, S. R., Shetter, R. E., Wert, B., Fried, A., Alicke, B., Stutz, J., Young, V. L., White, A. B., and Zamora, R. J.: OH and HO₂ concentrations, sources, and loss rates during the Southern Oxidants Study in Nashville, Tennessee, summer 1999, *Journal of Geophysical Research: Atmospheres*, 108, 4617–4634, doi:10.1029/2003JD003551, 2003.
- Mauldin, R. L., Cantrell, C. A., Zondlo, M., Kosciuch, E., Eisele, F. L., Chen, G., Davis, D., Weber, R., Crawford, J., Blake, D., Bandy, A., and Thornton, D.: Highlights of OH, H₂SO₄, and methane sulfonic acid measurements made aboard the NASA P-3B during Transport and Chemical Evolution over the Pacific : NASA global tropospheric experiment transport and chemical evolution over the Pacific (TRACE-P): Measurements and analysis (TRACEP1), *Journal of geophysical research*, 108, GTE17.1–GTE17.13, <http://cat.inist.fr/?aModele=afficheN&cpsid=15353084>, 2003.

- McDuffie, E. E., Edwards, P. M., Gilman, J. B., Lerner, B. M., Dubé, W. P., Trainer, M., Wolfe, D. E., Angevine, W. M., deGouw, J., Williams, E. J., et al.: Influence of oil and gas emissions on summertime ozone in the Colorado Northern Front Range, *Journal of Geophysical Research: Atmospheres*, 121, 8712–8729, 2016.
- Monge, M. E., D’Anna, B., Mazri, L., Giroir-Fendler, A., Ammann, M., Donaldson, D., and George, C.: Light changes the atmospheric reactivity of soot, *Proceedings of the National Academy of Sciences*, 107, 6605–6609, 2010.
- Müller, M., Mikoviny, T., Feil, S., Haidacher, S., Hanel, G., Hartungen, E., Jordan, A., Märk, L., Mutschlechner, P., Schottkowsky, R., Sulzer, P., Crawford, J. H., and Wisthaler, A.: A compact PTR-ToF-MS instrument for airborne measurements of volatile organic compounds at high spatiotemporal resolution, *Atmospheric Measurement Techniques*, 7, 3763–3772, doi:10.5194/amt-7-3763-2014, <http://www.atmos-meas-tech.net/7/3763/2014/>, 2014.
- 10 Olson, J., Prather, M., Berntsen, T., Carmichael, G., Chatfield, R., Connell, P., Derwent, R., Horowitz, L., Jin, S., Kanakidou, M., Kasibhatla, P., Kotamarthi, R., Kuhn, M., Law, K., Penner, J., Perliski, L., Sillman, S., Stordal, F., Thompson, A., and Wild, O.: Results from the Intergovernmental Panel on Climatic Change Photochemical Model Intercomparison (PhotoComp), *J. Geophys. Res.*, 102, 5979–5991, doi:10.1029/96JD03380, <http://onlinelibrary.wiley.com/doi/10.1029/96JD03380/abstract>, 1997.
- Osthoff, H. D., Roberts, J. M., Ravishankara, A. R., Williams, E. J., Lerner, B. M., Sommariva, R., Bates, T. S., Coffman, D., Quinn, P. K., 15 Dibb, J. E., Stark, H., Burkholder, J. B., Talukdar, R. K., Meagher, J., Fehsenfeld, F. C., and Brown, S. S.: High levels of nitryl chloride in the polluted subtropical marine boundary layer, *Nature Geosci*, 1, 324–328, doi:10.1038/ngeo177, <http://www.nature.com/ngeo/journal/v1/n5/full/ngeo177.html>, 2008.
- Paulot, F., Crounse, J., Kjaergaard, H., Kroll, J., Seinfeld, J., and Wennberg, P.: Isoprene photooxidation: new insights into the production of acids and organic nitrates, *Atmospheric Chemistry and Physics*, 9, 1479–1501, 2009.
- 20 Rabitz, H. and Alis, O. F.: General foundations of high-dimensional model representations, *Journal of Mathematical Chemistry*, 25, 197–233, doi:10.1023/A:1019188517934, <http://link.springer.com/article/10.1023/A%3A1019188517934>, 1999.
- Ren, X., Harder, H., Martinez, M., Leshner, R. L., Oligier, A., Simpas, J. B., Brune, W. H., Schwab, J. J., Demerjian, K. L., He, Y., Zhou, X., and Gao, H.: OH and HO₂ Chemistry in the urban atmosphere of New York City, *Atmospheric Environment*, 37, 3639–3651, doi:10.1016/S1352-2310(03)00459-X, 2003.
- 25 Ren, X., Brune, W. H., Cantrell, C. A., Edwards, G. D., Shirley, T., Metcalf, A. R., and Leshner, R. L.: Hydroxyl and Peroxy Radical Chemistry in a Rural Area of Central Pennsylvania: Observations and Model Comparisons, *J Atmos Chem*, 52, 231–257, doi:10.1007/s10874-005-3651-7, <http://link.springer.com/article/10.1007/s10874-005-3651-7>, 2005.
- Ren, X., van Duin, D., Cazorla, M., Chen, S., Mao, J., Zhang, L., Brune, W. H., Flynn, J. H., Grossberg, N., Lefer, B. L., Rappenglück, B., Wong, K. W., Tsai, C., Stutz, J., Dibb, J. E., Thomas Jobson, B., Luke, W. T., and Kelley, P.: Atmospheric oxidation chemistry 30 and ozone production: Results from SHARP 2009 in Houston, Texas, *Journal of Geophysical Research: Atmospheres*, 118, 5770–5780, doi:10.1002/jgrd.50342, 2013.
- Riedel, T. P., Wagner, N. L., Dub, W. P., Middlebrook, A. M., Young, C. J., Öztürk, F., Bahreini, R., VandenBoer, T. C., Wolfe, D. E., Williams, E. J., Roberts, J. M., Brown, S. S., and Thornton, J. A.: Chlorine activation within urban or power plant plumes: Vertically resolved ClNO₂ and Cl₂ measurements from a tall tower in a polluted continental setting, *J. Geophys. Res. Atmos.*, 118, 8702–8715, doi:10.1002/jgrd.50637, <http://onlinelibrary.wiley.com/doi/10.1002/jgrd.50637/abstract>, 2013.
- 35 Riedel, T. P., Wolfe, G. M., Danas, K. T., Gilman, J. B., Kuster, W. C., Bon, D. M., Vlasenko, A., Li, S.-M., Williams, E. J., Lerner, B. M., Veres, P. R., Roberts, J. M., Holloway, J. S., Lefer, B., Brown, S. S., and Thornton, J. A.: An MCM modeling study of nitryl chloride

- (ClNO₂) impacts on oxidation, ozone production and nitrogen oxide partitioning in polluted continental outflow, *Atmos. Chem. Phys.*, 14, 3789–3800, doi:10.5194/acp-14-3789-2014, <http://www.atmos-chem-phys.net/14/3789/2014/>, 2014.
- Roberts, J. M., Osthoff, H. D., Brown, S. S., Ravishankara, A. R., Coffman, D., Quinn, P., and Bates, T.: Laboratory studies of products of N₂O₅ uptake on Cl⁻ containing substrates, *Geophys. Res. Lett.*, 36, L20 808, doi:10.1029/2009GL040448, <http://onlinelibrary.wiley.com/doi/10.1029/2009GL040448/abstract>, 2009.
- Rohrer, F., Bohn, B., Brauers, T., Brüning, D., Johnen, F.-J., Wahner, A., and Kleffmann, J.: Characterisation of the photolytic HONO-source in the atmosphere simulation chamber SAPHIR, *Atmos. Chem. Phys.*, 5, 2189–2201, doi:10.5194/acp-5-2189-2005, 2005.
- Rolph, G.: READY - Real-time Environmental Applications and Display sYstem, <http://ready.arl.noaa.gov>: Accessed 3 Jan. 2016., 2016.
- Sander, S., Abbatt, J., Barker, J., Burkholder, J., Friedl, R., Golden, D., Huie, R., Kolb, C., Kurylo, M., Moortgat, G., Orkin, V., and Wine, P.: Chemical Kinetics and Photochemical Data for Use in Atmospheric Studies, Evaluation No. 17, JPL Publication 10-6, <http://jpldataeval.jpl.nasa.gov>, 2011.
- Saunders, S. M., Jenkin, M. E., Derwent, R. G., and Pilling, M. J.: Protocol for the development of the Master Chemical Mechanism, MCM v3 (Part A): tropospheric degradation of non-aromatic volatile organic compounds, *Atmospheric Chemistry and Physics*, 3, 161–180, doi:10.5194/acp-3-161-2003, <http://www.atmos-chem-phys.net/3/161/2003/>, 2003.
- Seinfeld, J. H. and Pandis, S. N.: *Atmospheric chemistry and physics: from air pollution to climate change*, John Wiley & Sons, 2012.
- Sheehy, P., Volkamer, R., Molina, L., and Molina, M.: Oxidative capacity of the Mexico City atmosphere–Part 2: A RO_x radical cycling perspective, *Atmospheric Chemistry and Physics*, 10, 6993–7008, 2010.
- Shirley, T., Brune, W., Ren, X., Mao, J., Leshner, R., Cardenas, B., Volkamer, R., Molina, L., Molina, M. J., Lamb, B., et al.: Atmospheric oxidation in the Mexico City metropolitan area (MCMA) during April 2003, *Atmospheric Chemistry and Physics*, 6, 2753–2765, 2006.
- Spencer, K., McCabe, D., Crounse, J., Olson, J., Crawford, J., Weinheimer, A., Knapp, D., Montzka, D., Cantrell, C., Hornbrook, R., et al.: Inferring ozone production in an urban atmosphere using measurements of peroxyacetic acid, *Atmospheric Chemistry and Physics*, 9, 3697–3707, 2009.
- Stein, A. F., Draxler, R. R., Rolph, G. D., Stunder, B. J. B., Cohen, M. D., and Ngan, F.: NOAA’s HYSPLIT Atmospheric Transport and Dispersion Modeling System, *Bull. Amer. Meteor. Soc.*, 96, 2059–2077, doi:10.1175/BAMS-D-14-00110.1, <http://journals.ametsoc.org/doi/10.1175/BAMS-D-14-00110.1>, 2015.
- Stemmler, K., Ammann, M., Donders, C., Kleffmann, J., and George, C.: Photosensitized reduction of nitrogen dioxide on humic acid as a source of nitrous acid, *Nature*, 440, 195–198, 2006.
- Stockwell, W. R., Kirchner, F., Kuhn, M., and Seefeld, S.: A new mechanism for regional atmospheric chemistry modeling, *Journal of Geophysical Research: Atmospheres*, 102, 25 847 – 25 879, doi:10.1029/97JD00849, 1997.
- Stone, D., Whalley, L. K., and Heard, D. E.: Tropospheric OH and HO₂ radicals: field measurements and model comparisons, *Chem. Soc. Rev.*, 41, 6348–6404, doi:10.1039/C2CS35140D, <http://dx.doi.org/10.1039/C2CS35140D>, 2012.
- Tan, Z., Fuchs, H., Lu, K., Hofzumahaus, A., Bohn, B., Broch, S., Dong, H., Gomm, S., Häsel, R., He, L., Holland, F., Li, X., Liu, Y., Lu, S., Rohrer, F., Shao, M., Wang, B., Wang, M., Wu, Y., Zeng, L., Zhang, Y., Wahner, A., and Zhang, Y.: Radical chemistry at a rural site (Wangdu) in the North China Plain: observation and model calculations of OH, HO₂ and RO₂ radicals, *Atmospheric Chemistry and Physics*, 17, 663–690, doi:10.5194/acp-17-663-2017, <http://www.atmos-chem-phys.net/17/663/2017/>, 2017.
- Thornton, J. A. and Abbatt, J. P. D.: N₂O₅ Reaction on Submicron Sea Salt Aerosol: Kinetics, Products, and the Effect of Surface Active Organics, *J. Phys. Chem. A*, 109, 10 004–10 012, doi:10.1021/jp054183t, <http://dx.doi.org/10.1021/jp054183t>, 2005.

- Thornton, J. A., Wooldridge, P. J., Cohen, R. C., Martinez, M., Harder, H., Brune, W. H., Williams, E. J., Roberts, J. M., Fehsenfeld, F. C., Hall, S. R., Shetter, R. E., Wert, B. P., and Fried, A.: Ozone production rates as a function of NO_x abundances and HO_x production rates in the Nashville urban plume, *Journal of Geophysical Research: Atmospheres*, 107, 7–17, doi:10.1029/2001JD000932, 2002.
- Thornton, J. A., Kercher, J. P., Riedel, T. P., Wagner, N. L., Cozic, J., Holloway, J. S., Dubé, W. P., Wolfe, G. M., Quinn, P. K., Middlebrook, A. M., Alexander, B., and Brown, S. S.: A large atomic chlorine source inferred from mid-continental reactive nitrogen chemistry, *Nature*, 464, 271–274, doi:10.1038/nature08905, <http://www.nature.com/nature/journal/v464/n7286/full/nature08905.html>, 2010.
- Tonnesen, G. S. and Dennis, R. L.: Analysis of radical propagation efficiency to assess ozone sensitivity to hydrocarbons and NO_x : 1. Local indicators of instantaneous odd oxygen production sensitivity, *Journal of Geophysical Research: Atmospheres*, 105, 9213–9225, doi:10.1029/1999JD900371, 2000.
- 10 Trainer, M., Parrish, D. D., Goldan, P. D., Roberts, J., and Fehsenfeld, F. C.: Review of observation-based analysis of the regional factors influencing ozone concentrations, *Atmospheric Environment*, 34, 2045–2061, doi:10.1016/S1352-2310(99)00459-8, <http://www.sciencedirect.com/science/article/pii/S1352231099004598>, 2000.
- Treadaway, V.: Measurement of Formic and Acetic Acid in Air by Chemical Ionization Mass Spectroscopy: Airborne Method Development, Master's thesis, University of Rhode Island, <http://digitalcommons.uri.edu/theses/603>, Paper 603, 2015.
- 15 Trebs, I., Bohn, B., Ammann, C., Rummel, U., Blumthaler, M., Königstedt, R., Meixner, F. X., Fan, S., and Andreae, M. O.: Relationship between the NO₂ photolysis frequency and the solar global irradiance, *Atmospheric Measurement Techniques*, 2, 725–739, doi:10.5194/amt-2-725-2009, <http://www.atmos-meas-tech.net/2/725/2009/>, 2009.
- US EPA: Laboratory study to explore potential interferences to air quality monitors, Govt. Doc. EP 4.52:2002006990, Office of Air Quality Planning and Standards, Research Triangle Park, NC Accessed online: 2014-01-04, 1999.
- 20 US EPA: Integrated Science Assessment of Ozone and Related Photochemical Oxidants(Final Report), Govt. Doc. EPA/600/R - 10/076F, Office of Research and Development, National Center for Environmental Assessment- RTP Division, Research Triangle Park, NC, 2013.
- US EPA: Ozone Trends, <https://www.epa.gov/air-trends/ozone-trends>, Accessed 22 April 2016., 2016a.
- US EPA: Ozone NAAQS | US EPA, https://www3.epa.gov/ttn/naaqs/standards/ozone/s_o3_index.html, 2016b.
- VandenBoer, T. C., Brown, S. S., Murphy, J. G., Keene, W. C., Young, C. J., Pszenny, A., Kim, S., Warneke, C., Gouw, J. A., Maben, J. R., et al.: Understanding the role of the ground surface in HONO vertical structure: High resolution vertical profiles during NACHTT-11, *Journal of Geophysical Research: Atmospheres*, 118, 2013.
- 25 VandenBoer, T. C., Young, C. J., Talukdar, R. K., Markovic, M. Z., Brown, S. S., Roberts, J. M., and Murphy, J. G.: Nocturnal loss and daytime source of nitrous acid through reactive uptake and displacement, *Nature Geoscience*, 8, 55–60, 2015.
- Wagner, N. L., Riedel, T. P., Young, C. J., Bahreini, R., Brock, C. A., Dubé, W. P., Kim, S., Middlebrook, A. M., Öztürk, F., Roberts, J. M., Russo, R., Sive, B., Swarthout, R., Thornton, J. A., VandenBoer, T. C., Zhou, Y., and Brown, S. S.: N₂O₅ uptake coefficients and nocturnal NO₂ removal rates determined from ambient wintertime measurements, *J. Geophys. Res. Atmos.*, 118, 9331–9350, doi:10.1002/jgrd.50653, <http://onlinelibrary.wiley.com/doi/10.1002/jgrd.50653/abstract>, 2013.
- Wainman, T., Weschler, C. J., Liou, P. J., and Zhang, J.: Effects of surface type and relative humidity on the production and concentration of nitrous acid in a model indoor environment, *Environmental Science & Technology*, 35, 2201–2206, PMID: 11414019, 2001.
- 35 Weibring, P., Richter, D., Fried, A., Walega, J., and Dyroff, C.: Ultra-high-precision mid-IR spectrometer II: system description and spectroscopic performance, *Applied Physics B*, 85, 207–218, 2006.
- Weibring, P., Richter, D., Walega, J. G., and Fried, A.: First demonstration of a high performance difference frequency spectrometer on airborne platforms, *Optics Express*, 15, 13 476–13 495, 2007.

- Wilson, K. L. and Birks, J. W.: Mechanism and elimination of a water vapor interference in the measurement of ozone by UV absorbance, *Environmental Science & Technology*, 40, 6361–6367, PMID: 17120566, 2006.
- Wolfe, G. M., Marvin, M. R., Roberts, S. J., Travis, K. R., and Liao, J.: The Framework for 0-D Atmospheric Modeling (FOAM) v3.1, *Geoscientific Model Development*, 9, 3309–3319, doi:10.5194/gmd-9-3309-2016, <http://www.geosci-model-dev.net/9/3309/2016/>, 2016.
- 5 Xue, L. K., Saunders, S. M., Wang, T., Gao, R., Wang, X. F., Zhang, Q. Z., and Wang, W. X.: Development of a chlorine chemistry module for the Master Chemical Mechanism, *Geosci. Model Dev.*, 8, 3151–3162, doi:10.5194/gmd-8-3151-2015, <http://www.geosci-model-dev.net/8/3151/2015/>, 2015.
- Zetzsch, C. and Behnke, W.: Heterogeneous Photochemical Sources of Atomic Cl in the Troposphere, *Berichte der Bunsengesellschaft physikalische Chemie*, 96, 488–493, doi:10.1002/bbpc.19920960351, <http://onlinelibrary.wiley.com/doi/10.1002/bbpc.19920960351/abstract>, 1992.
- 10 Zheng, W., Flocke, F. M., Tyndall, G. S., Swanson, A., Orlando, J. J., Roberts, J. M., Huey, L. G., and Tanner, D. J.: Characterization of a thermal decomposition chemical ionization mass spectrometer for the measurement of peroxy acyl nitrates (PANs) in the atmosphere, *Atmospheric Chemistry and Physics*, 11, 6529–6547, doi:10.5194/acp-11-6529-2011, <http://www.atmos-chem-phys.net/11/6529/2011/>, 2011.
- 15 Zhou, X., Gao, H., He, Y., Huang, G., Bertman, S. B., Civerolo, K., and Schwab, J.: Nitric acid photolysis on surfaces in low-NO_x environments: Significant atmospheric implications, *Geophysical Research Letters*, 30, 2217—2221, doi:10.1029/2003GL018620, 2003.
- Zhou, X., Zhang, N., TerAvest, M., Tang, D., Hou, J., Bertman, S., Alaghmand, M., Shepson, P. B., Carroll, M. A., Griffith, S., et al.: Nitric acid photolysis on forest canopy surface as a source for tropospheric nitrous acid, *Nature Geoscience*, 4, 440–443, 2011.

Table 1. Measured parameters input into the RACM2 and MCMv331. Inorganic chemical species measurement time resolution is 1 min. Aircraft chemical species were measured every 1 s. Evacuated whole-air canister VOC point measurements were interpolated to 1-h medians as described in Section 2.2. All measured constraints were either averaged or interpolated to 10 min for model runs.

Number	Model input	Method ^b	Uncertainty (%)	Institution
8	Inorganics			
	O ₃	CL	10	EPA
	SO ₂	UV Fluorescence	10	
	NO ₂ , NO	CES/CAPS, CL	10	
	CO, CO ₂ , CH ₄	WACs/GC/GC-MS (Colman et al., 2001)	≤ 5	UCI
	HNO ₃	TD-LIF (Day et al., 2002)	25	UC Berkeley ^a
58	Organic Species			
42	<i>C₂-C₁₀ NMHCs</i> ,	WACs/GC/GC-MS (Colman et al., 2001)	3-100	UCI
	<i>organic nitrates</i> :			
	ethane, ethene, acetylene, propane, propene, i-butane, n-butane, i-pentane, n-pentane, isoprene, n-hexane, n-heptane, n-octane, 2,3-dimethylbutane, 2-methylpentane, 3-methylpentane, 2,4-dimethylpentane, 2,2,4-trimethylpentane, cyclopentane, methylcyclopentane, cyclohexane, methylcyclohexane, benzene, toluene, ethylbenzene, m,p-xylene, o-xylene, 2-ethyltoluene, 3-ethyltoluene, 4-ethyltoluene, 1,3,5-trimethylbenzene, 1,2,4-trimethylbenzene, 1,2,3-trimethylbenzene, α -pinene, β -pinene, methyl nitrate, ethyl nitrate, i-propylnitrate, 2-butylnitrate, 2-pentylnitrate, 3-pentylnitrate, 2-methyl-2-butylnitrate			
	<i>NMHCs^a</i> :	PTR-ToF-MS (Müller et al., 2014)	10	U. Innsbruck
	methyl ethyl ketone, methanol, methyl vinyl ketone, methacrolein, acetic acid acetaldehyde, acetone formaldehyde	DFGAS (Weibring et al., 2006, 2007)	5	CU-INSTAAR
	peroxyl acetyl nitrate, peroxyl propyl nitrate	PAN-CIMS (Zheng et al., 2011)	13	NCAR
	hydrogen peroxide, formic acid, acetic acid	PCIMS (Treadaway, 2015)	30	URI
	ethanol, d-limonene/3-carene, camphene	TOGA (Apel et al., 2003)	30	NCAR

^a Denotes aircraft measurements

^b CL, chemiluminescence; CES, cavity enhanced spectroscopy; CAPS, cavity attenuated phase shift spectrometer; WAC, whole-air canister; GC, gas chromatography; GC-MS, gas chromatography mass spectrometer; TD-LIF, thermal dissociation laser-induced fluorescence; PTR-ToF-MS, proton transfer reaction time-of-flight mass spectrometer; DFGAS, difference frequency generation absorption spectrometer; CIMS, chemical ionization mass spectrometer ('PAN', peroxyacyl nitrate; 'P', peroxide); TOGA, trace organic gas analyzer.

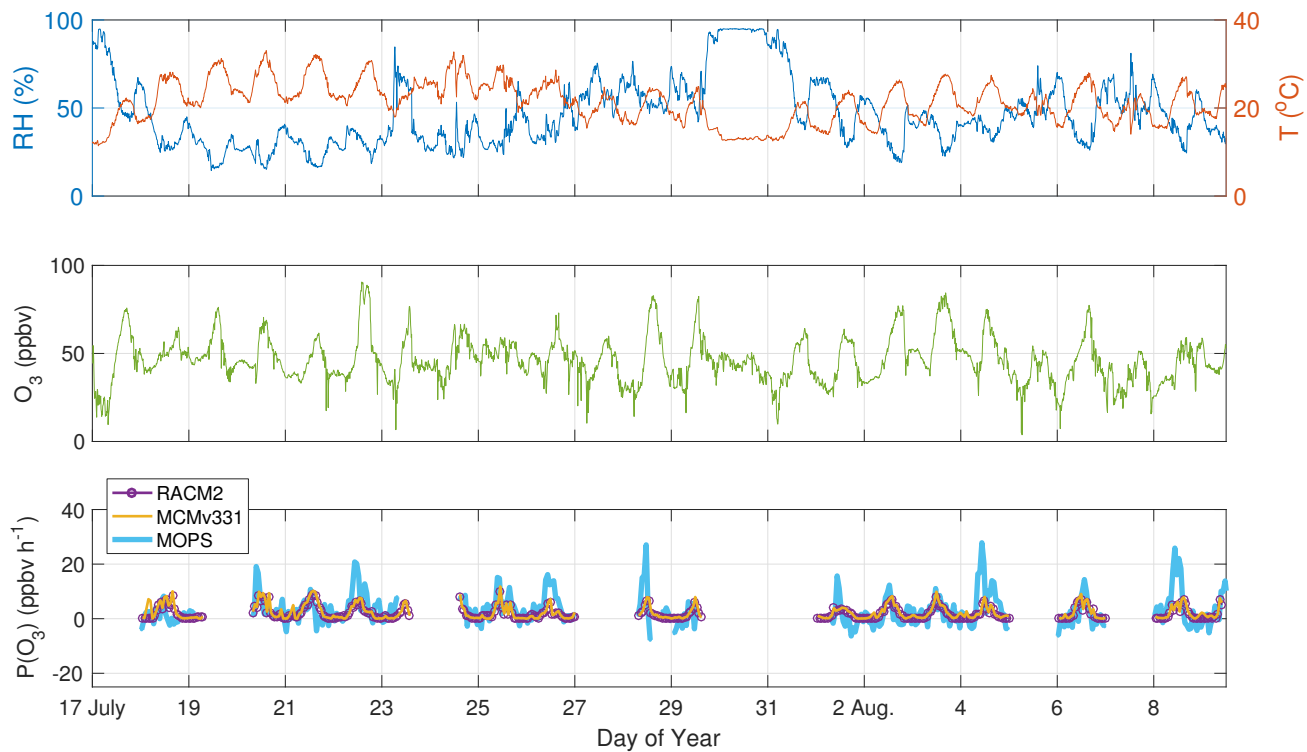


Figure 1. Top: Full-campaign 10-minute temperature and relative humidity in Golden, CO. The “warm” period is defined as days before 27 July 2014. Middle: Full-campaign 10-min O₃ mixing ratios for 17 July to 10 August 2014. Bottom: P(O₃) measured by the MOPS and modeled from the RACM2 and MCMv331 for the same time period. Measured to modeled comparisons are shown for days with available MOPS measurements and are averaged over a 1-hour time period.

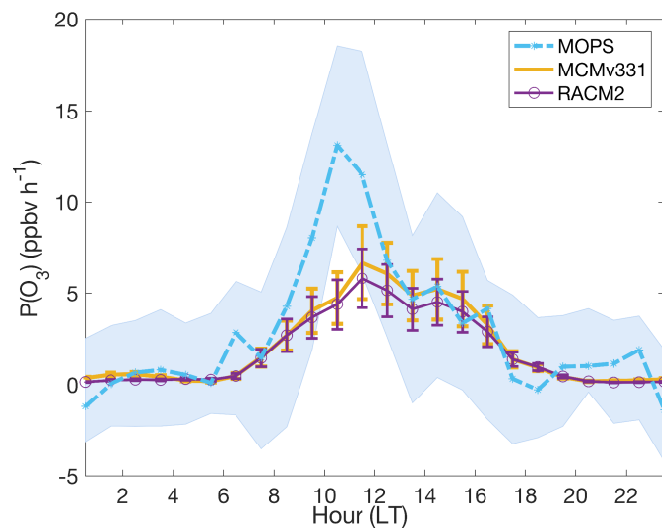


Figure 2. Full-campaign median hourly $P(O_3)$ measured by the MOPS, and modeled by the RACM2 and MCMv331 for MOPS measurement days. Shaded areas represent the variance in MOPS $P(O_3)$ due to the variation in the zero correction. The RACM2 and MCMv331 relative error bars are shown at the 1σ confidence level.

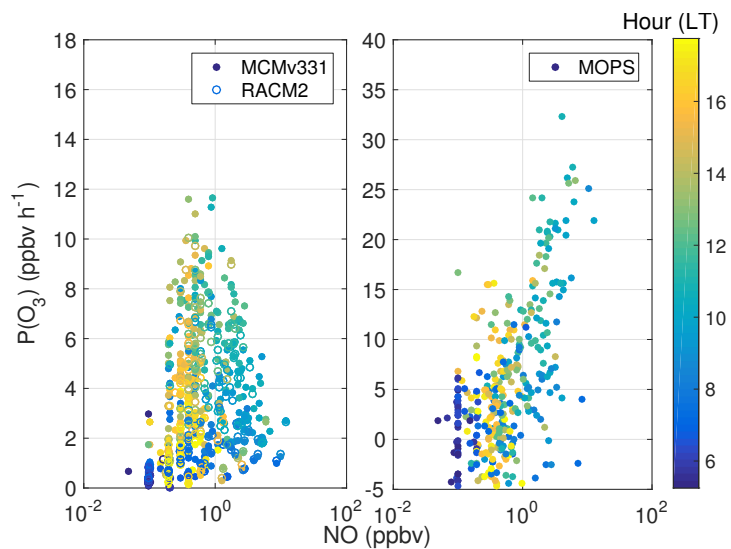


Figure 3. RACM2, MCMv331 (left), and MOPS (right) 30-minute $P(O_3)$ as a function NO for all MOPS measurement days. Points are colored by hour of day from 0600-1800 LT.

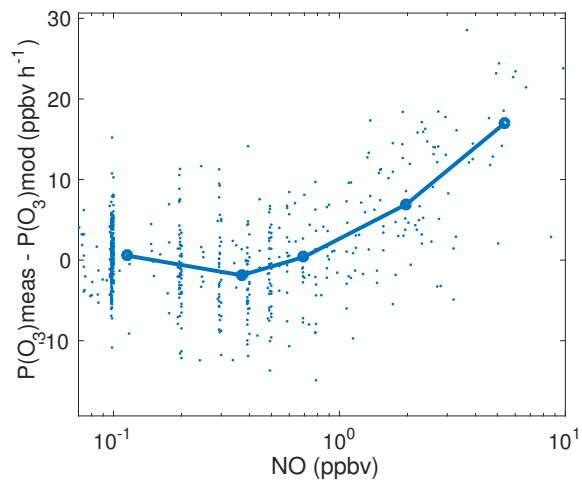


Figure 4. Difference between $P(O_3)$ measured and modeled as a function of measured NO. Individual points are averaged for 30 minutes, while the solid line indicates the average $P(O_3)$ difference binned by NO.

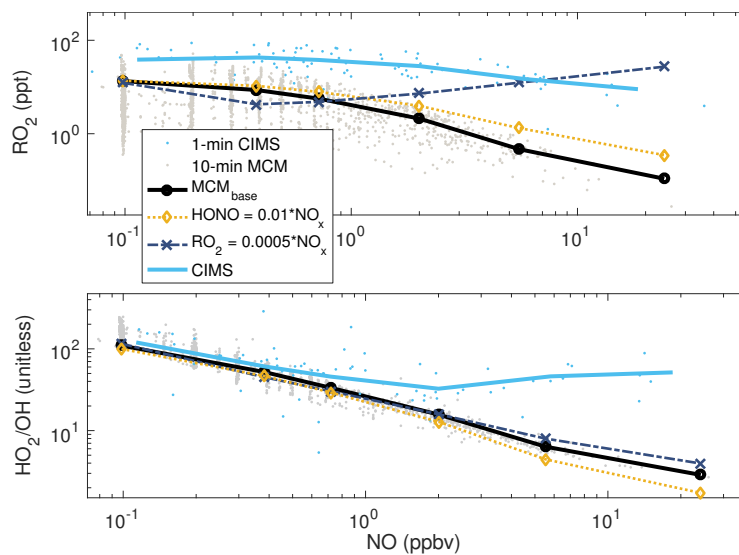


Figure 5. C-130 CIMS HO_2/OH ratio and RO_2 as a function of aircraft NO (chemiluminescence, $20 \text{ pptv} \pm 10\%$, 1σ uncertainty) and modeled HO_2/OH ratio and RO_2 versus constrained NO measured continuously in Golden, CO. Aircraft measurements used are limited to the first 1 km in the boundary layer and for only times when the C-130 was within 20 km of Golden, CO. A well-mixed boundary layer is assumed for all measurements.

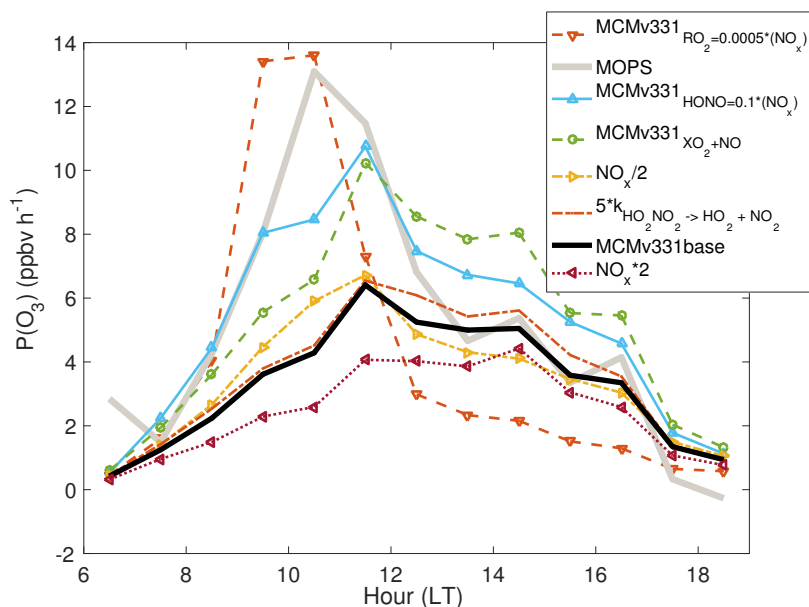


Figure 6. Model $P(O_3)$ scenarios using MCMv331 calculated for daytime $P(O_3)$ hours between 0600 and 1800 LT. Median hourly $P(O_3)$ is derived from the model case studies described in the main text and compared to the MOPs median diel $P(O_3)$ and MCMv331 median diel base case.

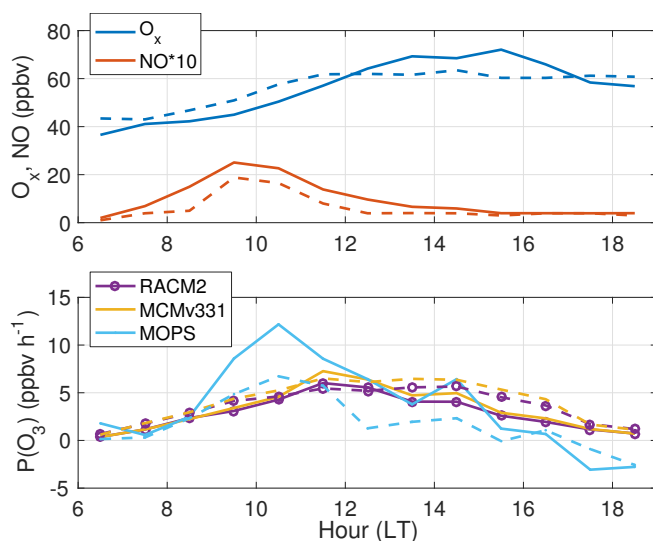


Figure 7. Top: O_x ($O_3 + NO_2$) and NO mixing ratios for Denver plume (solid) versus all other days (dashed) from 17 July - 10 August 2014 in Golden, CO. Bottom: Median measured and modeled $P(O_3)$ for Denver plume (solid) and non-Denver plume (dashed) days between 0600-1800 LT.